CRHyME (Climatic Rainfall Hydrogeological Model Experiment): a new model for geo-hydrological hazard assessment at the basin scale

Andrea Abbate[1], Leonardo Mancusi[1], Francesco Apadula[1], Antonella Frigerio[1], Monica Papini[2], Laura Longoni[2]

[1]RSE, Ricerca Sistema Energetico, Via Rubattino 54, Milano
5   [2]Politecnico di Milano, Piazza Leonardo da Vinci 32, Milano

Correspondence to: Andrea Abbate (andrea.abbate@rse-web.it)

Abstract. This work presents the new model CRHyME (Climatic Rainfall Hydrogeological Modelling Experiment), a tool for ~~the~~ geo-hydrological hazard evaluation. CRHyME is a physically based and spatially distributed model written in Python language that ~~and~~ represents an extension of the classic hydrological models working ~~that simulate inflows outflows~~ at the
10 basin scale. CRHyME's main focus is t~~A series of routines have been integrated to describe t~~he simulation of rainfall-induced ~~phenomena of~~ geo-hydrological instabilities such as shallow landslides as well as debris flows, catchment erosion, and sediment transport into the river. These phenomena are ~~generally~~ conventionally decoupled with respect to ~~a~~the continuous hydrological simulation while in CRHyME they are ~~quantitatively and~~ simultaneously and quantitatively evaluated within the same code through a multi-hazard approach.
15 CRHyME has been tested on some case studies in Italian basins. The Caldone catchment, a well-monitored basin of 27 km^2 located near Lecco city (Lombardy), was considered for the calibration of solid transport routine testing also the spatial scale dependence with respect to digital terrain resolution. CRHyME was applied across larger basins of the Valtellina and Emilia's areas (~2600 km^2) which have experienced in the recent past severe episode of geo-hydrological instabilities triggered by heavy precipitation. ~~were considered for the calibration and validation procedures of the model thanks also to the availability~~
20 ~~of literature data concerning past occurred geo-hydrological instability phenomena.~~ CRHyME's ~~Calibration and~~ validation ~~of the model conducted on presented case studies~~ ha~~ve~~s been assessed through some hydrological indexes NSE (Nash–Sutcliffe Efficiency) and RMSE (Root Mean Square Error) while for landslide phenomena the ROC (Receiver Operating Characteristic) methodology was applied. CHRyME has been able to: 1) reconstruct the surface runoff at the reference hydrometric stations located at the outlets of the basins, 2) estimate the solid transport at some hydropower reservoirs compared to the reference
25 data, and 3) evaluate the triggering conditions of shallow landslides and debris flows. ~~compared to those recorded in the literature.~~ The good performance ~~ranking~~ of CRHyME in terms of realistic reproduction of these catchment-scale effects ~~has shown a rather good performance of the model in terms of~~was reached assuring the stability of the code, a rather fast computation, and maintaining the numerical conservativity of water and sediment balances. CRHyME has reveale~~d~~s therefore a suitable tool for geo-hydrological process quantification, answering the recent needs of their numerical simulation not only
30 for back analysis studies but also useful for Civil Protection multi-hazard assessment.
~~, revealing suitable not only for back-analysis studies but also as an efficient tool for Civil Protection multi-hazard assessment.~~

1 Introduction

Landslides, floods, and debris flows represent serious geo-hydrological hazards in mountain environments (Gariano and Guzzetti, 2016). Among them, shallow landslide and debris flow failures are controlled by rainfall-triggering events of varying intensity and duration (Abbate et al., 2021a) while soil erosion and sediment transport are hydrologically driven processes occurring at catchment scale (Brambilla et al., 2020; Papini et al., 2017; Longoni et al., 2016; Ballio et al., 2010). Na(Brambilla et al., 2020; Papini et al., 2017; Longoni et al., 2016; Ballio et al., 2010)Shallow landslides and debris flows are often the result of soil erosion and sediment transport (Brambilla et al., 2020; Papini et al., 2017; Longoni et al., 2016; Ballio et al., 2010) and they can build up over long timescales due to the intermittency of mass wasting processes controlled by rainfall triggering events of varying intensity and duration (Abbate et al., 2021a). Natural disasters are a critical issue in terms of economic losses and causalities (ISPRA, 2018). Only in 2020, the worldwide losses related to geohazard were quantified as 210 billion dollars and 8'200 victims (Munich Re, 2021). Among the natural disasters, the events linked to geo-hydrological phenomena, such as floods and landslides, certainly play a significant role. In Italy, a total area of 50'117 km^2, which corresponds to 16.6% of the national territory is affected by high or very high landslide hazards and/or by a medium hydraulic hazard (ISPRA, 2018). In 2021, the number of victims of landslide and flood events were was five and the evacuated people were around 1'000 (CNR and IRPI, 2021). Northern Italy has the highest mortality rate caused by landslides and floods (number of deaths and missing people per 100'000 people in one year) in the country, varying in the range of 0.034 for Emilia Romagna and 0.085 for Piedmont.

Geo-hydrological hazards are complex and heterogeneous phenomena, so a great deal of effort has been made in the past to try and interpretunderstand their dynamics and triggering factors (Gariano and Guzzetti, 2016; Ceriani et al., 1994; Gao et al., 2018; Kim et al., 2020). There are many studies concerning shallow landslide dynamics in the literature-based both on laboratory and field experiments (Guzzetti et al., 2007; Herrera, 2019; Meisina et al., 2013; Crosta et al., 2003; Iverson, 2000; Ivanov et al., 2020b), which individuate highlight rainfall as the main triggering factor for this type of phenomenon. However, in the literature is still missing a widely accepted methodology that can strongly connect strongly the different components that have an interplay role in geo-hydrological hazards generation and evolution (Gariano and Guzzetti, 2016; Bordoni et al., 2015). In this context, shallow landslides, debris flow and solid transport are primarily driven by superficial soil water balance that can also influences the runoff generation through the infiltration mechanisms (Abbate et al., 2019).

In this work, the potentialities of a new physically-based geo-hydrological model called CRHyME are illustrated. CRHyME is an extension of a classical rainfall-runoff hydrological model where also geo-morphological dynamic aspects are taken into account. From the analysis of the literature (De Vita et al., 2018; Bemporad et al., 1997; Roo et al., 1996; Schellekens et al., 2020; Angeli et al., 1998; Gleick, 1989; Sutanudjaja et al., 2018; Van Der Knijff et al., 2010; Devia et al., 2015; Moges et al., 2021), rarely the two aspects have been jointly analysedtaken into account. Lots of hydrological models, adopted worldwide are interested mainly in flood propagation and water balance assessment (Sutanudjaja et al., 2018). One of their main limitations is that they are rather advanced in the hydrological part, proposing a very detailed description of the hydrological

65   cycle while geo-hydrological hazards interaction is barely taken into account (Shobe et al., 2017; Strauch et al., 2018). Up to now, there are still few examples that can include the triggering analysis of shallow landslide and debris flow, or a solid transport quantification (Roo et al., 1996; Gariano and Guzzetti, 2016; Alvioli et al., 2018). In literature, some examples consider the erosion and solid transport mechanisms at the watershed scale (Vetsch et al., 2018; Tangi et al., 2019; Roo et al., 1996; Papini et al., 2017) while the stability of natural slopes is still not properly included in distributed hydrological models

70   and vice-versa. The slope stability or debris flow analysis is computed inside dedicated models such as those (Iverson, 2000; Scheidl and Rickenmann, 2011; Harp et al., 2006; Milledge et al., 2014; Montrasio, 2008; Takahashi, 2009) that takes into account some aspect of the hydrological cycle but they are generally not fully integrated into a rainfall-runoff routine. Moreover, several models can be applied to a few cases~~have limiting spectra of application mainly~~ due to several limitations such as input data requirements, the scale of simulation and the data resolution (Devia et al., 2015; Moges et al., 2021).

75   Fortunately, some advances in this direction have been made in very recent years. In this regard, CHASM (Combined Hydrology and Stability Model) (Bozzolan et al., 2020) and Landlab (Strauch et al., 2018) represent the two latest modelling frameworks that have addressed the need to start evaluating the geo-hydrological hazard and risks considering also hydrological and ~~climatical~~ climatic aspects. The new methodological approaches shown by CHASM and Landlab models have been assessed thanks to the progressively increasing data availability for GIS (Geographical Information Systems) on a

80   worldwide scale and thanks to the recent improvements in computer programming for environmental systems. Indeed, the creation of efficient and open-source built-in functions for different language programs, such as Matlab, C++ or Python, has sped up and facilitated the implementation of self-made ~~earth~~land--surface models. These functions have been already successfully implemented by PCR-GLOBWB-2 (Sutanudjaja et al., 2018) and WFLOW (Schellekens et al., 2020) models, as well as in the European hydrological model LISFLOOD (Van Der Knijff et al., 2010) and OPENLISEM (Roo et al., 1996).

85   ~~Starting from these considerations and taking inspiration from these models, the first version of CRHyME was developed.~~ The main motivations aimed at the construction of the new CRHyME code are here presented:

- Versatility and integrated modelling of the rainfall-induced geo-hydrological process (flood, erosion, sediment transport and shallow landslide triggering);
- Fast and efficient simulations within a spatially distributed model designed to operate at catchment scale without

90   constraints on spatial and temporal input data resolution;
- Code implementation inside a robust framework, using Opens Source Python libraries which enable fast coding and easy sub-modules modifications/integrations;
- Code compatibility for assimilating input data from Opens Source datasets available at a worldwide scale, permitting a simulation reproducibly in whatever catchments;

95   Starting from these considerations and taking inspiration from ~~these~~analogue models cited before, CRHyME (Figure 1) was developed to try to fill the existing gaps and issues, improving overall geo-hydrological modelling. This paper presents the main features and several applications of the ~~CRHyME model~~code. Structure and constitutive equations are reported in the

3

Material and Method section. Then ~~the~~ some case studies developed across Italian territory ~~waerere~~ taken into account for the calibration and validation of the new model. In the Result sections the main outcomes of CRHyME applications are reported and they are extensively commented on within the Discussion and Conclusions sections.
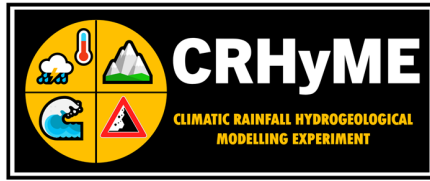

Figure 1: CRHyME logo.

2 Material and Methods

In this paragraph, the CRHyME model peculiarities are illustrated: the main features, the sub-module structure and their constitutive equations, the input dataset for its initialization, and a presentation of the test cases study. ~~(Figure 1), created for a correct quantification of the hazard deriving from floods and landslides at basin scale.~~

2.1 Model main features ~~CRHyME's engine is based on PCRaster libraries (Karssenberg et al., 2010; Pebesma et al., 2007) which is a collection of open-source software targeted at the development and deployment of spatio-temporal environmental models. These functions can include a rich set of model building blocks and analytical functions for manipulating raster GIS maps, a framework for the construction of stochastic spatio-temporal models and a tool for interactive visualisation of spatio-temporal data. They are mainly applied in environmental modelling such as rainfall-runoff models and slope stability models and can deal with spatially distributed earth surface data that are discretized considering the single cell of terrain domain as the reference element where model calculations are carried out. Using PCRaster libraries, 4 different processes that describe quantitatively the geo-hydrological hazards that may occur at the catchment scale have been implemented:~~

~~• River flow discharge and volume;~~

~~• River erosion and sediment transport discharge and volume;~~

~~• Shallow landslide triggering condition;~~

~~• Debris flow triggering condition.~~

~~The most innovative part of the code~~ CRHyME aims to model together hydrological and geological processes occurring at the catchment scale, e.g. floods and landslides. Historically, these processes have been studied separately but in CRHyME are evaluated simultaneously: ~~are strongly connected and they usualincludes the physical relations that describe how the hydrological assessment can influence and potentially trigger the geo-hydrological hazards occurring at the basin scale:~~

4

125 the bed-load sediment transport in terms of the bed-load process has been described considering the Erosion Potential Method (EPM) for simulating erosion processes sources (Longoni et al., 2016; Brambilla et al., 2020; Milanesi et al., 2015; Ivanov et al., 2020a) and the stream power laws available in the literature for defining the transport capacity of the rivers (Vetsch et al., 2018) : the sFor what concerns shallow landslide failure assessment, slope stability models commonly adopted in engineering geology have been implemented to evaluate the stability conditions of natural slopes was carried out considering 4 infinite-

130 slope stability models (Iverson, 2000; Montrasio, 2008; Harp et al., 2006; Milledge et al., 2014);. T the selection of the stability model depends on the number and type of landslides (e.g., deep-seated, shallow), the type and amount of information available to characterize the slope or landslide, and the extent of the study area (e.g., a single slope or landslide, a catchment, a large geographical region). In CRHyME, we were interested mainly in the simulation of the shallow landslide. the debris flow stability was evaluated through the theory proposed by (Takahashi, 2009) since, according to (Theule, 2012; Jakob and Jordan,

135 2001), , defining a rigid boundary between flood, solid transport, debris flow and shallow landslide processes is not always possible. they are complex phenomena which reside in the middle so defining a unique criterion for analysing their instability cannot be assessed straightforwardly since they can behave intermediately among floods and landslides.

The aim was to merge the potentiality of the reference models cited before : including a well-organized model framework, already adapted to work with meteorological reanalysis and climate scenarios data (PCR-GLOBWB-2), predicting and

140 quantifying some geo-hydrological processes (Landlab and CHASM), and extending the event-based simulation (OPENLISEM) to a continuous simulation over a longer period. The CRHyME's code architecture is partially inherited by the PCR-GLOBWB-2 model (Sutanudjaja et al., 2018). This model is characterized by a well-organized model framework that could guarantee the robustness and the stability of the code, fast modelling and reduced time consuming thanks to embedded function parallelization, no constraints on the spatial and temporal resolution of the input data, and easy code adaptation for

145 new features. The PCR-GLOBWB-2 engine is based on PCRaster libraries (Karssenberg et al., 2010; Pebesma et al., 2007). The PCRaster Python libraries offer a series of standard functions prepared for hydrological processing on calculation grids which can be easily "called" via Python scripts to perform individual operations. CRHyME's framework is organized within a modular structure which enables easier single-model updating to introduce new features. Python programming language is open-source, and its flexibility permits to manage of large meteorological and climatic databases which are essential for

150 computing extending the event-based simulation (OPENLISEM) to a continuous simulation over a longer period and long-term simulations. Alle these features has been included, adapted, reworked, and improved inside CRHyME. CRHyME's engine is based on PCRaster libraries (Karssenberg et al., 2010; Pebesma et al., 2007) which is a collection of open-source software targeted at the development and deployment of spatio-temporal environmental models. These functions can include a rich set of model building blocks and analytical functions for manipulating raster GIS maps, a framework for the construction of

155 stochastic spatio-temporal models and a tool for interactive visualisation of spatio-temporal data. They are mainly applied in environmental modelling such as rainfall-runoff models and slope stability models and can deal with spatially distributed earth surface data that are discretized considering the single cell of terrain domain as the reference element where model calculations are carried out. Using PCRaster libraries,
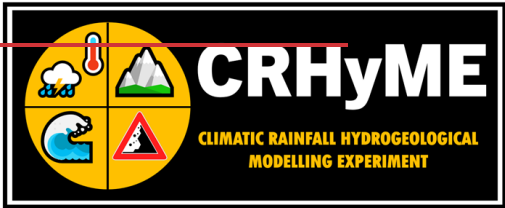
5

160

Figure 1: CRHyME logo.

2.2 Model sStructure

The CRHyME model is composed of a series of modules connected in a time-loop as represented in Figure 2. The simulations are initialized from a pre-compiled ".INI" file (see the aAppendix A) where all the settings and input data paths are specified (see the Appendix B). The modules are:

In the .INI file are essentially reported the simulation time settings (e.g. starting date and ending date), the spatially distributed input data and the meteorological and climatological data series, the settings of each computational module and the name of the output files. The .INI file is read by the "deterministic_runner.py" file that starts the CRHyME model and its internal routines. Except for "pre-processing.py", "reporting.py" and "plot.py" modules, where variables are respectively defined, saved, and plotted following the formats and standards of the PCRaster libraries (Sutanudjaja et al., 2018; Karssenberg et al., 2010), other modules contain the physical equations that aim to simulate the geo-hydrological cycle.

1. CLIMA: elaborates precipitation and temperature data from reanalysis and climate datasets, using the "NetCDF" (Network Common Data Form, ".netcdf") format (Bonanno et al., 2019; Sutanudjaja et al., 2018);

2. METEO: elaborates precipitation and temperature data from ground-bases weather stations using the PCRaster standard format ".tss" (Karssenberg et al., 2010) for data series and calculates the evapotranspiration;

3. INTERCEPTION + SNOW: excludes from net precipitation the canopy interception and the snow;

4. LANDSURFACE: evaluates the water balance in the superficial soil giving information about runoff, soil moisture and percolation losses;

5. GROUNDWATER: evaluates the water balance in the groundwater layer;

6. ROUTING: calculates the runoff routing across the watershed;

6

185   7. LANDSLIDE: identifies the triggering conditions for landslides, and debris flows and calculates erosion and
        bed-load sediment transport in rivers.

The first 6 modules constitute the "hydrological module" and are deputed for assessing the hydrological cycle while the "landslide module" is the CRHyME's novelty that individuates slope instability conditions and simulates sediment transport considering respectively the computed soil moisture and runoff. CRHyME's timestep required for completing a single loop of

190 all internal modules (Figure 2) is assumed to be equal to the meteorological forcings timestep and could vary from a minimum of 5 min up to a maximum of 1 day. In this current work, the timestep selected for CRHyME's computations is 1 day.

Figure 1: Framework and modules of the new model CRHyME. For further details see Appendix A and B.

195

The PCRaster libraries implemented in CRHyME have the advantages to be fully parallelized to work with multicore processors (Karssenberg et al., 2010). This is an important aspect of our code that permits us to decrease sharply the time-consuming of each simulation. The intrinsic parallelization of the PCRaster libraries simplifies and facilitates code maintenance and updating, without any further parallelization optimizations. In Table 1 the operating time calculation ranked

200 for the model CRHyME is reported for different numbers of core processors (workers).

	PCRaster N° Workers	Single Operation with a large file (10'000 cells)	Single Cycle of model Iteration
2 cores	2	4.07 s	Around 20 – 25 s
4 cores	4	1.48 s	Around 8 – 10 s
8 cores	8	1.05 s	Around 5 – 6 s

Table 1: Performances of the CRHyME model working on different CPU core sets. It can be noticed that by increasing the number of cores available, the computation time for a particular operation can drop significantly.

2.2.1 Model initialization

The choice of a suitable digital terrain model (DTM or DTM) is used in CRHyME as a the fundamental starting point for the computationsCRHyME's code. From DTM all the essential data listed in the ".INI" file are derivedall the essential data listed at the beginning of the .INI file required for hydrological operations using PCRaster libraries: the "clone.map", a 0-1 mask that defines the computational domain; the "ldd.map", the local drain direction map that defines the flow directions (Karssenberg et al., 2010; Pebesma et al., 2007). In CRHyME, the is provided by HydroSHEDS DTM (Hydrological data and maps based on SHuttle Elevation Derivatives at multiple Scales) (Lehner et al., 2008) was selected as a reference. The is provided by HydroSHEDS DTM is designed specifically for hydrological models (Lehner et al., 2008) and has been already pre-processed to guarantee the flow connectivity of the river network (hydrologically conditioned). Its spatial resolution is about 3-sec degree, which corresponds approximately to about 90 m at the equator, and it was retained sufficiently accurate for catchment scale analysis. Using the PCRaster functions, the hydrographic network, the '. Moreover, slope', the 'curvature' and the 'slope aspect' were reconstructed immediately from HydroSHED DTM. In addition to these morphologicaly data, other layers are required in CRHyME for the geo-hydrological assessment are:

- the Corine Land Cover data (https://land.copernicus.eu) (Girard et al., 2018), was considered for defining vegetation interception and soil infiltration coefficients, spatial evapotranspiration flux and root cohesion for landslide stability;
- the Soil Grids data at 250 m resolution from the world database ISRIC — World Soil Information (https://maps.isric.org/) (Hengl et al., 2017), were considered for assessing soil physical properties such as depth and soil composition which are implemented inside infiltration, percolation, erosion and landslide stability routines;
- the hydraulic properties of soils, such as the permeability and porosity, from the European and global databases (https://esdac.jrc.ec.europa.eu/) (Tóth et al., 2017; Ross et al., 2018; Huscroft et al., 2018), were considered for assessing superficial and groundwater hydrological balance.

The datasets here described (Figure 3) are freely available freely for the entire European area, but analogous can be found for other continents. Since they are provided with an open-source licence they can be implemented without restrictions. This choice aims to extend and generalise as much as possible the reproducibility of CRHyME's simulations in whatever worldwide catchments without any constrain on territorial input data. Moreover, the availability of free Web Feature Service (WFS) and Web Coverage Service (WCS) services allows one to download them easilydown, speeding up . It will be included in the future version of the model as a CRHyME pre-processorinitialization.

Temperature and rainfall data required by simulations were gathered from ground-based meteorological stations (Rete Monitoraggio ARPA Lombardia; Rete Monitoraggio ARPA Emilia) and reanalysis databases available locally (Bonanno et al., 2019). Temperature fields were built by combining the data series at each timestep, estimating the regression coefficient with respect to the station elevation and then using the DTM information to distribute temperature spatially (Daly et al., 1997; Chow et al., 1988). For rain gauge precipitation, as simple IDW (Inverse Weight Distance) interpolator was implemented with a distance exponent equal to 2 while for rainfall data coming reanalysis data, a simple nearest-neighbour algorithm has been

adopted to downscale the precipitation field at DTM resolution (Daly et al., 1997; Chow et al., 1988; Abbate et al., 2021b; Terzago et al., 2018).
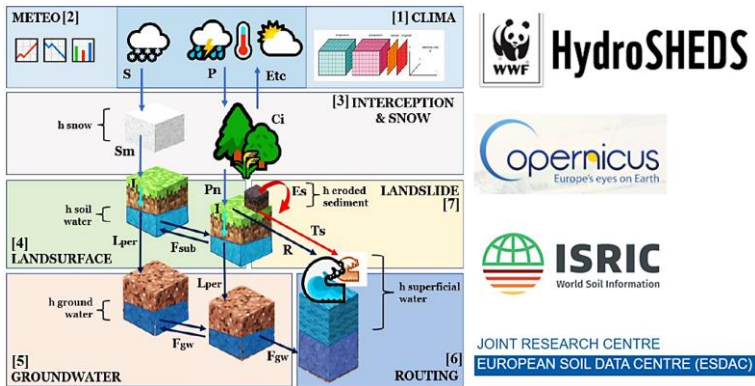
An automatic procedure that allows extracting all the required territorial data at the catchment scale has been built up in
240   Python to facilitate the elaborations. It connects directly to WFS and WCS services of the cited databases downloading the data required. It will be included in the future version of the model as a CRHyME pre-processor.

Figure 2: Scheme of the terrain water and sediment balances and related mass-fluxes in CRHyME and the input datasets.

(Jacob et al., 2014; Sutanudjaja et al., 2018)

245   **2.2.2 Hydrological module and equations**

The hydrological modules (Figures 2 and 3, from 1 to 6) evaluate the processes of transformation inflows-outflows using input maps of weather forcings consisting of precipitation [$mm\,timestep^{-1}$] and average, maximum, and minimum temperature [$C°$]. In CRHyME The model also calculates evapotranspiration losses ETc(t) according to two formulations chosen by the user: Hargreaves and Pennman-Montheit, both taken from FAO guidelines (Raziei and Pereira, 2013; Allan et al., 1998).
250   Although during intense precipitation events the evapotranspiration portion can often be neglected (Chow et al., 1988), its calculation is essential for continuous long-term hydrological simulations. Moreover, this is important also for short-term simulations because may influence the initial conditions of the soil moisture $S_m(t)$ (Abbate et al., 2019; Lazzari et al., 2018; Mostbauer et al., 2018). each cell of the terrain domain is considered like a tank that communicates in cascade to the others following the downstream river network (Brambilla et al., 2020; Roo et al., 1996; Sutanudjaja et al., 2018). Hydrological
255   balance is schematized considering 4 imaginary layers where water can be temporarily stored:

      1. Snow Storage, Eq. (1) where snow balance assessed by $h_{snow}(t)$ variable, [mm],

9

2. Superficial Soil Storage, Eq. (2) and (3) where infiltration is computed and superficial soil balance is assessed by $h_{soilwater}(t)$ variable, [mm],

3. Groundwater Soil Storage, Eq. (5) where groundwater balance is assessed by $h_{groundwater}(t)$ variable, [mm],

4. Runoff Storage, Eq. (6) where runoff generated by an excess of infiltration and exfiltration is routed across the catchment and described by $h_{runoff}(t)$, [mm].

4.

Superficial soil storage is the core of hydrological balance assessment since is the place where all the water mass fluxes, in [mm timestep^{-1}], are exchanged between atmosphere and terrain. Balances are is schematized by Eq.(1), Eq. (2) and Eq. (3) and the fluxes in this layer are evaluated [mm timestep^{-1}]. Canopy Interceptions $C_r(t)$:

• Infiltration I(t): that is the part of the volume that enters the soil using two of the most common infiltration models Horton and SCS-CN (Chow et al., 1988; Chen and Young, 2006; Mishra et al., 2003; Morbidelli et al., 2018; Ravi et al., 1998; Smith and Parlange, 1978; Ross et al., 2018); Canopy Interceptions $C_r(t)$: that is the part of the rainfall intercepted by trees leaves;

• Snowmelt $S_{ml}(t)$ and Snow S(t): the melted snow coming from the snowpack;

• Infiltration I(t): that is the part of the volume that enters the soil using two of the most common infiltration models Horton and SCS-CN (Chow et al., 1988; Chen and Young, 2006; Mishra et al., 2003; Morbidelli et al., 2018; Ravi et al., 1998; Smith and Parlange, 1978; Ross et al., 2018);

▪ Infiltration balance in Eq. (2) establishes the net water volume I(t) that enters the soil. From precipitation P(t) is evaluated by the net precipitation $P_n(t)$ arriving at the terrain surface subtracting the part of the rainfall intercepted by tree leaves, e.g. Canopy Interceptions $C_I(t)$ (Li et al., 2017; Nazari et al., 2019). When the temperature is $< 0°C$, all the precipitation is stored as snowpack $h_{snow}(t)$ Eq. (1) and released aftermath as snowmelt contribute $S_{ml}(t)$ when temperature increases above 0 following a degree days approach (Chow et al., 1988; Cazorzi and Dalla Fontana, 1996). I(t) is estimated directly using the common infiltration methods of Horton and SCS-CN (Chow et al., 1988; Chen and Young, 2006; Mishra et al., 2003; Morbidelli et al., 2018; Ravi et al., 1998; Smith and Parlange, 1978; Ross et al., 2018) and the runoff generated by an excess of precipitation at the surface R(t), is obtained by the difference of $P_n(t) - I(t)$:

▪ Superficial soil moisture balance in Eq. (3) permits to evaluate of the quantity $S_m(t)$ which is expressed adimensional as a ratio between $h_{soilwater}(t)$ [mm] and the product of terrain porosity n and the superficial soil depth (depth$_{Soil}$). Porosity and superficial soil depth are determined respectively from (Tóth et al., 2017; Ross et al., 2018; Huscroft et al., 2018) and (Hengl et al., 2017) databases. The other terms of the water balance are:

o ETc(t) evapotranspiration losses according to Hargreaves and Pennman-Montheit formulations suggested by FAO guidelines (Raziei and Pereira, 2013; Allan et al., 1998)

10

- $L_{per}(t)$ percolation losses are ~~the~~ part of the volume that goes to the ~~deepest~~ groundwater layer, evaluated as a function of the soil water balance in unsaturated conditions using Van Genucten's functions and parameters (Jie et al., 2016; Van Genuchten, 1980; Daly et al., 2017; Groenendyk et al., 2015; Vitvar et al., 2002; Jackson et al., 2014; Klaus and Jackson, 2018);

  o Exfiltration $Ex(t)$ ~~and $Ex_{GW}(t)$~~ is the leakage of water on the surface that occurs after the complete saturation of the superficial soil storage (ponding);

  o $F_{sub}(t)$ is the sub-surface lateral fluxes generated inside the superficial soil layer through the Dupuit approximation of the Darcy law for water filtration in soils. Here is a correction of the saturated permeability Ks [m s^{-1}] considering the relative permeability Kr [-] caused by the partial saturation conditions has been included in the formula (Van Genuchten, 1980).

- ~~(groundwater) following the complete saturation of the soil (aquifer) column.~~
- ~~$F_{sub}(t)$ and $F_{GW}(t)$: lateral fluxes generated inside superficial soil layer and groundwater layer, following the Dupuit law for unsaturated — saturated soils.~~
- ~~$F_{kin-dyn}(t)$: runoff fluxes computed using the kinematic or dynamic flow routing PCRaster functions.~~

~~All the fluxes related to water mass balance are converted to the standard international units such as [$m^3 s^{-1}$] for discharges while storage quantities $\Delta h_{snow}(t)$, $\Delta h_{soilwater}(t)$, $\Delta h_{groundwater}(t)$ and $\Delta h_{runoff}(t)$ are converted into [m^3] for volumes. $S_m(t)$ is expressed in [mm] and converted to adimensional quantity [$-$] if divided by product of the terrain porosity n and height.~~

$$\frac{dh_{snow}(t)}{dt} \cong \frac{\Delta h_{snow}(t)}{\Delta t} = S(t) - S_{ml}(t)$$	(1)
$$I(t) = P(t) - C_I(t) + -S_{ml}(t) - R(t) = P_n(t) - R(t)$$	(2)
$$\frac{dS_m(t)depth_{Soil}n}{dt} S_m(t) = \frac{dh_{soilwater}(t)}{dt} \cong \frac{\Delta h_{soilwater}(t)}{\Delta t} = I(t) - ETc(t) - Ex(t) - L_{per}(t) \pm F_{sub}(t)$$	(3)

The groundwater reservoir depth ($depth_{GW}$) has been modelled considering a spatial distribution described in Eq. (4) (Fan et al., 2007; de Graaf et al., 2015a; Pelletier et al., 2016). According to these studies, as the superficial slope increases, the aquifer depth is reduced until it reaches the minimum value of 0 m, e.g., corresponding to the condition of complete absence.

$$depth_{GW} = a/(1 + b * slope)$$	(4)

In Eq. (4) the slope is expressed as a tangent to the angle of inclination of the surface while a and b represent coefficients that are distinguished according to the depths of interest: In the case where the depth of the bedrock is contained, the parameter a

= 20 and b = 125; In case the depth of the bedrock is more important, regolith condition, the parameter a = 120 and b = 150. In CRHyME a rather intermediate condition has been adopted between superficial bedrock and regolith present, therefore the parameters adopted are the following: a = 200 and b = 125. This approximation has appeared sufficiently accurate concerning the fact that currently available data on groundwater aquifer depth and hydrogeology parameters are rather approximated and uncertain (Kobierska et al., 2015; Zomlot et al., 2015; Hayashi, 2020; Huscroft et al., 2018).

$$\frac{dh_{groundwater}(t)}{dt} \cong \frac{\Delta h_{groundwater}(t)}{\Delta t} = L_{per}(t) - Ex_{GW}(t) \pm F_{GW}(t) \qquad (45)$$

The groundwater table is generated by the percolated water $L_{per}(t)$ coming from the upper layer Eq. (5). The groundwater lateral flow $F_{GW}(t)$ is then calculated using the Dupuit approximation according to which the filtration rate is given by the product of hydraulic permeability Ks for the tangent of the slope of the impermeable substrate, supposed parallel to the slope (Klaus and Jackson, 2018; Anderson, 2005; Bresciani et al., 2014). $Ex_{GW}(t)$ e.g., groundwater exfiltration, is the term that describes the leakage of water after the complete saturation of the groundwater storage, simulating the water springs.

$$\frac{dh_{runoff}(t)}{dt} \cong \frac{\Delta h_{runoff}(t)}{\Delta t} = R(t) + Ex(t) + Ex_{GW}(t) \pm F_{kin-dyn}(t) \qquad (6)$$

$$\frac{dh_{runoff}(t)}{dt} \cong \frac{\Delta h_{runoff}(t)}{\Delta t} = R(t) + Ex(t) + Ex_{GW}(t) \pm F_{kin-dyn}(t) \qquad (5)$$

S

At the groundwater reservoir, the sub-surface flow is generated thanks to the percolated water from the upper layer Eq. (4). The flow is calculated using the Dupuit approximation according to which the filtration rate is given by the product of hydraulic permeability for the tangent of the slope of the impermeable substrate, supposed parallel to the slope (Klaus and Jackson, 2018; Anderson, 2005; Bresciani et al., 2014). The sub-surface flow has been modelled considering a special distribution of the groundwater depth (Fan et al., 2007; de Graaf et al., 2015; Pelletier et al., 2016). This approximation has appeared sufficiently precise concerning the fact that up to now available data on groundwater aquifer depth and hydrogeology parameters are rather approximated and uncertain with respect to the affordability of the superficial layers data (Kobierska et al., 2015; Zomlot et al., 2015; Hayashi, 2020; Huscroft et al., 2018).

uperficial runoff is defined as the sum of $R(t)$, $Ex(t)$ and $Ex_{GW}(t)$ and it is stored in $h_{runoff}(t)$ in Eq. (6). $h_{runoff}(t)$ The sum of the surface and the emerged sub-surface runoffs areis propagated across the overland surface, along the lines of maximum slope and inside, the river network using two possible methods available in PCRaster libraries that are deputed for the flow routing process (Chow et al., 1988; Lee and Pin Chun, 2012; Collischonn et al., 2017; Bancheri et al., 2020); kinematic and dynamic $-F_{kin-dyn}(t)$. Both derived from the simplification of De Saint Venant's one-dimensional equations of motion. The first is generally used applied in sections where the slopes are accentuated so it is possible to approximate the hydraulic gradient with the slope of the channel (Chow et al., 1988). The second instead introduces further terms that allow a better simulation of the outflow in correspondence to the flat areas where when the other terms of the De Saint Venant equation are no longer

negligible (Chow et al., 1988), but requires precise information about the geometry of rivers sections to carry out the flood
wave propagation (Karssenberg et al., 2010).

2.2.3 Geo-hydrological module and equations

In order tTo study geo-hydrological instability it is of paramount importance to analyse the triggering causes of landslides and
the dynamic of erosion processes (Guzzetti et al., 2005; Remondo et al., 2005; Montrasio and Valentino, 2016; Bovolo and
Bathurst, 2012). For this purpose, an ad hoc new "landslide module" (Figure 3, n° 7) has been developed in CRHyME.

2.2.3.1 Stability models for shallow landslides and debris flows

Shallow landslides triggering is strongly correlated with meteorological and climatic forcing (Abbate et al., 2021a). The abrupt
modification of the local hydrology due to the alternation of dry and wet conditions of soil induced by precipitation is
responsible for undermining the stability of the slopes (Iverson, 2000; Chen and Young, 2006). Here are described briefly the
four stability models included in CRHyME: 1) Iverson model (Iverson, 2000), Eq. (7), 2) Harp model (Harp et al., 2006), Eq
(8), 3) Milledge model (Milledge et al., 2014) and, Eq (9), 4) SLIP model (Montrasio, 2008; Montrasio and Valentino, 2016),
Eq. (10). The one-dimensional theory considers the hypothesis of an infinitely extended slope where the stability is guaranteed
by the safety factor (FS), defined as the ratio between the resistant forces compared to the mobilizing ones. This model theory
is based on the concept of limit equilibrium of the inclined plane for which the weight component of the specific gravity γ_s
parallel to the slope, having a slope α, is destabilizing while the friction force allows the ground to remain in balance. In
CRHyME, the one-dimensional model was implemented by imagining each cell as a slope element for which the value of the
safety factor FS is calculated. Typical values of the friction angle and cohesion for superficial terrains have been obtained from
literature references, while the water content is the result of the hydrological balance carried out by hydrological modules.
According to the principle of effective stress, as the soil moisture increases, normal efforts are reduced by an aliquot equal to
the pressure generated by the water itself (Iverson, 2000).

$$FS = \frac{\tan(\varphi)}{\tan(\alpha)} - \frac{\psi\gamma_w\tan(\varphi)}{\gamma_s Z \sin(\alpha)\cos(\alpha)} + \frac{c}{\gamma_s Z \sin(\alpha)\cos(\alpha)}$$	(7)
$$FS = \frac{\tan(\varphi)}{\tan(\alpha)} + \frac{m\gamma_w\tan(\varphi)}{\gamma_s \tan(\alpha)} + \frac{c}{\gamma_s Z \sin(\alpha)}$$	(8)
$$FS = \frac{2F_{rl} + F_{rb} + F_{rd} - F_{du}}{F_{dc}}$$	(9)
$$FS = \frac{N'\tan\varphi + C'}{W'\sin\alpha + F'}$$	(10)

The key parameters of the Iverson Eq. (7) and Harp model Eq. (8) are essentially 3: the friction angle φ [°] and the cohesion of the soil c [kPa] which are a function of the terrain granulometry and the superficial soil moisture $S_m(t)$. In~~side~~ Iverson's model is described by the hydraulic load of the local aquifer $\psi = f(S_m(t))$, expressed in [kPa], while inside the Harp model is described by the variable $m = \frac{S_m(t)}{z}$, expressed in [-]. Milledge model Eq. (9) considers not only the friction effects along the sliding surface F_{rb} expressed in [N], but also the cut resistance along the side walls F_{rl} in [N], the passive force of the upstream terrain F_{du}, in [N], the active force of the valley terrain F_{rd} in [N], and the mobilizing force due to the terrain weight F_{dc}, in [N]. In the SLIP model Eq. (10) the terms are expressed in [N]: N' is the normal component of the weight as a function of porosity n and soil moisture $S_m(t)$; C' is the cohesion term; W' is the slope parallel component of the weight as a function of porosity n and soil moisture $S_m(t)$; F' is the term that expresses the seepage forces that are related to the presence of the temporal water table. Since ~~at catchment scale~~ slopes are vegetated, two other factors should be included: the additional cohesion of the root system of trees and the additional weight of plant biomass (Cislaghi et al., 2017; Yu et al., 2018; Rahardjo et al., 2014). In ~~fact~~As a matter of fact, in the absence of radical cohesion, those portions ~~areas were~~ are perpetually in conditions of instability with FS < 1. The addition of root cohesion, varying between 1 – 10 kPa depending on the tree species and the type of land use, has made it possible to correct the estimates of the stability ~~model~~stability evaluation.

A debris flow represents an eventually huge movement of mass that can be triggered on steep slopes and travel_s_ long distances reaching the fan of the watershed outlet (Takahashi, 2009). These events are set intermediately between shallow landslides, where the solid behaviour is prevalent, and floods where liquid rheology is the driving force (Iverson et al., 1997). Therefore, solid concentration within the saturated deposit and the presence of superficial water flowing above are the key parameters for assessing the triggering condition. As can be appreciated by ~~the~~ Eq. (~~10~~11) and (~~11~~12), two criteria are at least to be included. The first one is derived from the theory of infinite slope stability where the solid concentration parameter C_* is included as the principal triggering factor. C_* is the grain concentration by volume in the static debris bed and can be expressed by the ratio between the soil content [m^3] in respect to the sum of the soil content and soil water volume [m^3]. Increasing the local water volume, the soil concentration starts to progressively reduce. The criterium requires the indication of soil density σ [kg m^{-3}], water density ρ [kg m^{-3}], the surface runoff height h [m] and the parameter a that can be assumed equal to the representative diameter of the soil deposit, such as D_{50}, expressed in [m]. The second criterium considers that a sufficient superficial runoff q_l above the debris flow deposit is present, expressed in [m^{3}s^{-1}].

$$FS_{debris} = \frac{\dfrac{C_*(\sigma - \rho)}{C_*(\sigma - \rho) + \rho\left(1 + \dfrac{h}{a}\right)}\tan\varphi}{\tan\theta}$$	(~~10~~11)
$q_* = q_l / \sqrt{D_{50}^{~3} * g} \geq 2$	(~~11~~12)

Debris flow deposits are generally constituted by incoherent material that is cohesionless (Iverson et al., 1997; Takahashi, 2009; Rickenmann, 1999). Therefore, if only the first criterion is applied, several catchments~~'s~~ will appear unrealistically

14

unstable because the cohesion is completely neglected. The second criterion is necessary because can reduce the basin portions susceptible to debris flow occurrence. When it heavy rains, the lateral impluvium may generate locally a high concentration of runoff fluxes that can saturate these deposits and trigger a debris flow (Theule, 2012).

400

2.2.32.2 Erosion production and bed-load solid transport evaluationrouting

Gavrilovic's method, also called Erosion Potential Method (EPM), was initially developed in southern ex-Yugoslavia and then successfully applied also in Switzerland and Italy, it is a semi-quantitative method capable of giving an estimation of erosion and sediment production in a basin (Longoni et al., 2016; Milanesi et al., 2015; Globevnik et al., 2003; Brambilla et al., 2020).

405 Eq. (1213) represents the synthesis of Gavrilovic's method. The average annual volume of eroded material G, expressed in $[m^3 yr^{-1}]$, is a product of W_s and R, which are respectively the average annual production of sediment due to surface erosion, expressed in $[m^3 yr^{-1}]$ Eq. (1314), and the retention coefficient, adimensional $[-]$ in Eq. (1415) considers the possible re-sedimentation of the eroded material across the watershed.

$$G = W_S R$$	(1213)
$$W_s = \pi H\cancel{H} \tau_G Z^{\frac{3}{2}} A$$	(1314)
$$R = \frac{\sqrt{OD}(l + l_{lat})}{(l + 10)A}$$	(1415)

410 The terms that appear in the equations are τ_G -temperature coefficient [°C], H average annual precipitation value $[mmyr^{-1}]$, Z erosion coefficient $[-]$, A basin area $[km^2]$, O perimeter of the basin [km], D average height of the basin [km], l length of the main water course [km], l_{lat} the total length of the lateral tributaries [km]. The values of Z are generally correlated to the land use characteristics and geological maps (Milanesi et al., 2015). The Gavrilovic method was developed to work with annual data of mean precipitation and temperature. Since with CRHyME, we are interested in a continuous simulation, the method

415 has been temporally downscaled substituting P and T at yearly bases with the time-step precipitation [mm timestep^{-1}] and temperature [C°].

Gavrilovic method defines W_s as the source of available sediment that can be routed through the watershed until the outlet. In CRHyME the solid routing has been modelled considering its strong relation with liquid discharge. First of all, t~~The latter is corrected by recalling the~~ theory of incipient motion of Shields that states the starting motion of sediments in the function of

420 D_{50} quantity (Chow et al., 1988; Merritt et al., 2003; Vetsch et al., 2018) is evaluatedimplemented (Figure 4). ~~In particular,~~ t~~Then~~he solid discharge is evaluated in two mannersways. A first calculation considers a ~~pure Transport Limited~~stream-power formula for bed load transport (Morgan and Nearing, 2011; Shobe et al., 2017; Campforts et al., 2020), where the solid discharge is expressed as a power-law function of the river channel slope and liquid discharge. ~~The latter is corrected by recalling the theory of incipient motion of Shields that states the starting motion of sediments in the function of D₅₀ quantity~~

425 ~~(Chow et al., 1988; Merritt et al., 2003; Vetsch et al., 2018).~~ A second calculation represents an adaptation of the kinematic

15

model for clear water to the sediment transport, under the strong hypothesis that the velocity of sediment transport is assumed ~~like~~ similar to the water flow. The application of the kinematic method requires the estimation of stage-discharge relations for the sediment in analogy with the clear water stage-discharge functions. Several authors (Govers, 1989; Govers et al., 1990; Rickenmann, 1999) have considered this hypothesis reasonable when no further additional information about solid transport is available. The first implementation of solid transport routing ~~and balance is founded on the hypothesis of~~is defined as Transport Limited (TL) ~~as a prevalent condition~~. Here, solid discharge, expressed in $[m^3 \, s^{-1}]$, is a function of the reach hydraulic and geometrical characteristics and it doesn't consider the local availability of the sediment in the channel that may decrease the amount of sediment delivered. The second one is representative of the Erosion Limited (EL) condition (Shobe et al., 2017; Campforts et al., 2020) where the ~~material available~~sediment availability in the river or on the slopes tends to limit effective water erosion, as it frequently happens. For this second case.~~In both cases,~~ the sediment balance has been assessed in each cell through Eq. (16) considering: the erosion rate ($E_s = W_s$) equal to the source term computed by Gavrilovic and the deposition rate (D_s) following (Shobe et al., 2017), expressed in $[m \, yr^{-1}]$; ~~and~~the transport term (T_s) considering the kinematic model adapted for sediment routing, expressed in $[m^3 \, s^{-1}]$; the sediment amount $h_{solid}(t)$ in $[m]$, converted in $[m^3]$ if multiplied by cell area extension $[m^2]$.~~, with Eq. (15).~~

$$\frac{dh_{solid}(t)}{dt} \cong \frac{\Delta h_{solid}(t)}{\Delta t} = D_s(t) - E_s(t) \pm T_s(t) \tag{16}$$

~~(Abeshu et al., 2021)In CRHyME both TL and EL methods are consideredare evaluated for solid transport assessment. According to (Papini et al., 2017; Ivanov et al., 2020a; Dade and Friend, 1998; Lamb and Venditti, 2016; Peirce et al., 2019; Pearson et al., 2017; Ancey, 2020), the sediment transport dynamic is an active research frontier. In this sense, the spatial distribution of D_{50} is a critical issue because is difficult to be reconstructed at catchment scale. Moreover, D_{50} distribution influences incipient motion threshold that sharply modify sensibly the local sediment routing leading to wrong estimations of the watershed sediment yield.~~

~~;empirical According to these authors, several morphological, climatic, hydrological, and geological factors can influence the river granulometry. Among them, slope-like factors have shown a quite significant correlation with D_{50} and in some cases sfound (Nino, 2002). formula D_{50}function Even though s represent a crude approximation it has a physical meaning since in the upper catchment (where slopes are steepness) coarse granulometries are prevalent while at the outlet (where slopes are lower) the sediment fine fraction becomes important. In CRHyME's model D_{50} is a necessary data, therefore a bunch of empirical slope — D_{50} curves have been implemented. Curve's parameters were calibrated ad hoc with respect to the available sediment yield measurements and on-site granulometry surveys conducted in the examined areas.~~
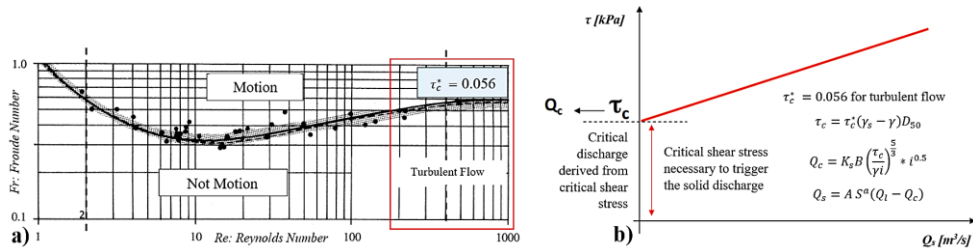
Figure 3: a) Shield abacus for solid transport incipient motion under different conditions of turbulence (Re number) and flow regime (Fr number). In the red box is defined the typical range of turbulent flow in rivers with a critical adimensional shear stress τ_c^* of 0.056; b) evaluation of the incipient motion condition for solid transport where the critical shear stress τ_c and the critical liquid discharge Q_c are a function of the local granulometry through the parameter D_{50}.

In CRHyME both TL and EL methods are simultaneously evaluated for assessing sediment transport yield within a physically reasonable range. According to (Papini et al., 2017; Ivanov et al., 2020a; Dade and Friend, 1998a; Lamb and Venditti, 2016; Peirce et al., 2019; Pearson et al., 2017; Ancey, 2020), the sediment transport dynamic is an active research frontier. In this sense, the spatial distribution of D_{50} is a critical point because is difficult to be reconstructed at the catchment scale (Abeshu et al., 2021). Moreover, D_{50} distribution influences incipient motion threshold that sensibly modifies the local sediment routing leading to wrong estimations of the watershed sediment yield. Since it doesn't exist a close formulation for indirectly estimating the granulometry in the absence of an on-field survey dataset, empirical approaches have been proposed by (Nino, 2002; Sambrook Smith and Ferguson, 1995; Lamb and Venditti, 2016; Berg, 1995). According to these authors, several morphological, climatic, hydrological, and geological factors can influence the river granulometry at particular section. Among them, slope-like factors have shown a quite significant correlation with D_{50} and in some cases $slope - D_{50}$ relations were retrieved (Nino, 2002). Namely, D_{50} tends to increase with steepness **slope**. These relations mimic the formula proposed by (Berg, 1995) where the D_{50} is indirectly determined using a power-law function describing the river morphology evolution. Even though $slope - D_{50}$ represent a crude approximation it has a physical meaning since in the upper catchment (where slopes are steepness) coarse granulometries are generally prevalent while at the outlet (where slopes are lower) the sediment fine fraction becomes more significant (Tangi et al., 2019). In CRHyME, the D_{50} is a necessary granulometric data, therefore an ensemble of empirical $slope - D_{50}$ curves have been included to assess automatically D_{50} distribution across the catchment using slope data. Curve's parameters were calibrated ad hoc in the examined areas comparing simulated sediment yields to the available measurements and with on-site granulometry surveys conducted.

17

485

In the recent literature, some simplified models of sediment erosion and transport have been proposed to fulfil the need to quantify these processes (Tangi et al., 2019; Bizzi et al., 2021; Czuba, 2018; Gilbert and Wilcox, 2020; Beveridge et al., 2020). The models described represent a strong idealization of what can happen at the catchment scale. Some authors have proposed a framework where the river network is discretized in "segments" where the mass balance of water and solid are assessed starting from the top

490 of the basin up to the outlet. These "topological" frameworks are fast and rather simple to interpret and have the peculiarity to include all the infrastructures, such as dams, that can perturb the sediment balance at reached levels (Tangi et al., 2019; Bizzi et al., 2021; Schmitt et al., 2018). One of their main worth points is the possibility to include statistical analysis on inputs and making Montecarlo iterations to reach the best accordance with monitoring field data. Montecarlo statistical technique is applied especially for assessing the granulometry of each reach of the catchment where the sediment source strongly depends on the characteristic

495 diameters (Tangi et al., 2019). In several cases, an automatic procedure has been implemented and rather large catchments have been studied (Bizzi et al., 2021; Schmitt et al., 2018). However, these models suffer from the same problems as the distributed ones: the scarcity of reference data that are necessary to select the more realistic Montecarlo simulation and the not complete understanding of the erosion-transport processes. According to (Beveridge et al., 2020; Sklar et al., 2017), the erosion processes on the hillslopes are rather complex and are difficult to conceptualize in a unique framework since several factors work together at

500 different scales and at different times to manipulate the soil granulometry. In particular, sediment delivery to river reaches depends on landslides that occurred in the past that are a barely random process without a characteristic of periodicity (Gilbert and Wilcox, 2020; Sklar et al., 2017). Moreover, several assumptions on transport dynamics are assumed in these models such as the hypothesis of equilibrium of the sediment supply across the rivers (Bizzi et al., 2021; Gilbert and Wilcox, 2020) that, in some cases, maybe not be representative of the real condition that is again barely unknown. Due to their simplicity, these models are generally not integrated

505 with a hydrological routine because are intended to focus only on sediment transport mechanisms (Bizzi et al., 2021; Gilbert and Wilcox, 2020; Beveridge et al., 2020). So, liquid discharge data series are required to be initialized and some hypothesis about uniform flow motion using Gauckler-Manning-Strickler formula are needed to associate a proper discharge value at eac2.2.3.3 Linking together geo-hydrological processes

The processes here described may occur simultaneously inside a catchment, especially during heavy rains or after periods of

510 prolonged precipitation (Abbate et al., 2021a). In CRHyME, the erosion and sediment transport are well integrated within the hydrological routines following the state-of-the-art of available model in the literature. Here, both the triggering function (sediment detachment and incipient motion) and the magnitude (amount of sediment eroded and transported) have been quantified. On the other side, for shallow landslide and debris flow, only the triggering condition of failure has been analysed while the mass wasting propagation across the catchment has not been included in the code yet. This choice is motivated by

515 the fact that mass wasting failures, especially for debris flows, are characterized by large uncertainties in their volume quantification related mainly to the entrainment processes but depending also on DTM spatial resolution (larger pixel = large volume amount) (Jakob and Hungr, 2005). The entrainment effect is difficult to be modelled in a closed form and the uncertainties described may perturb the volume estimation by orders of magnitude (D'Agostino and Marchi, 2001). Mass

18

wasting processes may have a strong incidence on sediment transport dynamic and compared to the widespread erosion, which

520 is a "low intensity" process, landslides may change abruptly the geo-morphological characteristics of the catchment.

2.3 Model performance

2.3.1 Hydrological iIndexes and sediment tTransport assessment and assessment

Assessing hydrological performance at basin outlets is evaluated through error indexes that compare water discharges recorded by the local hydrometer and the water discharge simulated by the model (Chow et al., 1988; Bancheri et al., 2020). The most

525 common indexes are Nash–Sutcliffe Efficiency (NSE), and Root-Mean-Square Error (RMSE). The Nash–Sutcliffe Efficiency (NSE) (Eq. 17) is a normalized model efficiency coefficient. It determines the relative magnitude of the residual variance compared with the measured data variance where S_i and M_i are the predicted and observed values at a given time step. The NSE varies from $-\infty$ to 1, where 1 corresponds to the maximum agreement between predicted and observed values. The Root-Mean-Square Error (RMSE) (Eq. 1718) is given by where M_i and S_i represent the measured and simulated time series,

530 respectively, and N is the number of components in the series.

$$NSE = 1 - \frac{\sum_{i=1}^{n}(S_i - M_i)^2}{\sum_{i=1}^{n}(M_i - \overline{M_i})^2}$$	(17)
$$RMSE = \sqrt{\frac{1}{N}\sum_{i=1}^{n}(M_i - S_i)^2}$$	(18)

For the sediment transport assessment, the periodical bathymetry campaigns carried out inside hydropower reservoirs can be considered as a reference (Pacina et al., 2020; Langland, 2009; Marnezy, 2008). With respect to hydrometric data which can be easily acquired from local environmental agencies (Rete Monitoraggio ARPA Lombardia; Rete Monitoraggio ARPA Emilia), bathymetries are generally not accessible to the public (ITCOLD, 2009, 2016). Therefore, the calibration and

535 validation of erosion and sediment transport models have considered the seasonal volume estimation in hydro plants reservoirs and the event-based volume estimation only where available. For the case studies analysed, these data were retrieved from specific reports (Milanesi et al., 2015; Ballio et al., 2010; Brambilla et al., 2020).

2.3.2 ROC curves for local landslide prediction

540 According to several authors (Formetta et al., 2016; Pereira et al., 2016; Vakhshoori and Zare, 2018; Gudiyangada Nachappa et al., 2019; Kadavi et al., 2018; Fawcett, 2006), a useful technique to assess the good prediction performances of a slope stability models is the Receiver Operating Characteristic (ROC) methodology. The ROC curve is a graphical plot that illustrates the diagnostic ability of a binary classifier system as its discrimination threshold is varied. In landslide stability assessment, the binary classificatory is the condition of FS $\geq$> 1 (stable) or FS < 1 (unstable) that each pixel of the model can

545 match in the function of the local morphology (slope), terrain characteristics and hydrological conditions (Formetta et al., 2016; Vakhshoori and Zare, 2018).

In CRHyME, ~~model doesn't build a susceptibility map but it simply counts~~ the number of ~~the~~ landslide activation~~s is counted~~. ~~On~~ on each timestep, a 0-1 map is produced ~~if the~~where the ~~instability condition~~destabilized pixels (~~of~~ FS < 1) are signed as 1 ~~is verified~~while stable pixels (FS ≥ 1) are signed with 0. The spatial scale where the activations are represented is dependent
550 on the pixel dimension of the HydroSHED DTM. ~~The spatial scale where the activations are represented is the pixel dimension of the HydroSHED DEM. This resolution may be sufficient to spot a single shallow landslide activation but there are uncertainties on its real extension that could be in principle lower or greater than single-pixel size.~~

According to (Harp et al., 2006), the inclusion of a "pixel-buffer" in the surrender area of a "pixel-based" shallow landslide failure is necessary to describe ~~more~~ physically the process ~~of~~ of ~~shallow landslide~~ activation. Generally speaking, landslide
555 instability areas are not confined to the landslide body but could extend to surrounding boundaries: in the upper part, the landslide crown could experiment with further collapse since other cracks may generate and propagate retrogressively (Ivanov et al., 2020b); in the bottom part, the landslide may evolve into soil slip or earth flow and travel along the slope following the maximum gradient (Jakob and Hungr, 2005); the lateral boundaries could be also affected by landslide instability due to shear stress perturbation and reduced lateral roots cohesion (Rahardjo et al., 2014) that develops during landslide collapsing.
560 Bearing in mind that a single-pixel evaluation may be ~~too reductive~~not conservative, in CRHyME the failure activation considers ~~also~~ a buffer around made by its 8 adjacent cells, as reported in Figure 5a. 9-pixel counting may overestimate in some cases the extension of the hazard area since this methodology is pixel scale-dependent. In our case, the 90 m resolution has been considered compatible since cross-validation has been done considering the typical dimension of a shallow landslide. A survey conducted looking at the Italian ~~landslide database~~catalogue (IFFI: Inventario Fenomeni Franosi Italiano) (ISPRA,
565 2018; Guadagno et al., 2003; Guzzetti and Tonelli, 2004) has shown that ~~where~~ the typical spatial extension of the shallow landslide is comprised of between 200^2 m^2 and 400^2 m^2. This result is compatible with the 9-pixel counting because the overall landslide extension $(90x3)^2$ m^2 falls within the catalogue range. This choice has also been motivated by the guideline for shallow landslide susceptibility mapping produced by (Harp et al., 2006). Since the reference data on historical landslides in the IFFI catalogue comes from several sources, the localization of the instability could not be georeferenced ~~geo-localized~~ with
570 high precision. ~~In order to carry out the ROC methodology~~To, avoid~~ing~~ these issues in reference data, a buffer zone with different radii around each landslide point was created: 250 m, 500 m, 1000 m and 2000 m (Figure 5). This radius represents an attempt for considering the uncertainties about the real position of the triggered landslide.

ha formattato: Apice
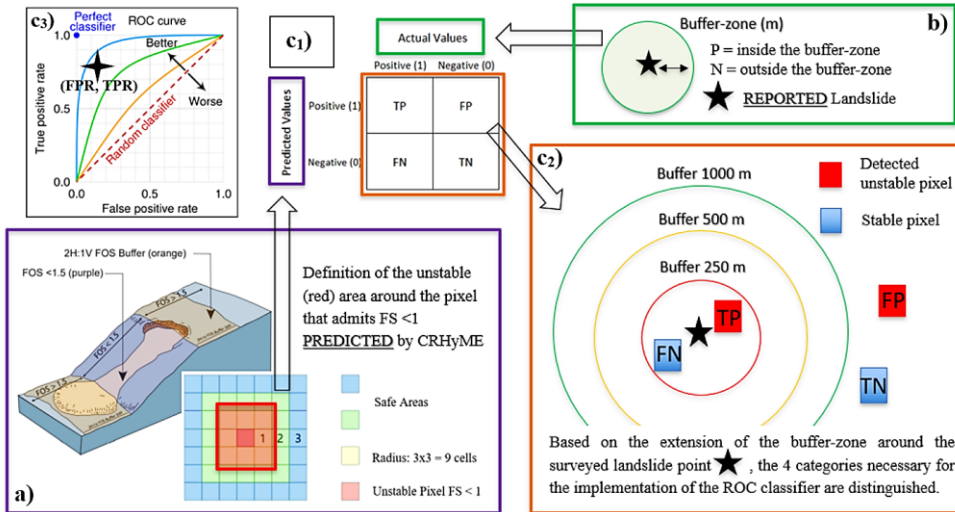
Figure 4: a) Extension of unstable pixel computed by model CRHyME considering the surrounded 8 cells, **b)** buffer-zones defined for each reference landslide point with different extensions and **c)** workflow of the ROC methodology: c1) confusion matrix, c2) ~~with the~~ evaluation of parameters TP, FN, TN and FP, in respect to the position of the buffer-zone around the reported landslide point. TP, FN, TN and FP change within the extension of the buffer zone, c3) graphical representation of the ROC curves and the (FPR, TPR) point.

$$FPR = \frac{FP}{N} = \frac{FP}{FP + TN} \qquad (19)$$

$$TPR = \frac{TP}{P} = \frac{TP}{TP + FN} \qquad (20)$$

Knowing the reference instabilities (retrieved by IFFI) and the predicted instabilities (coming from CRHyME simulations), the ROC assessment was conducted to rank the ability of CRHyME in detecting the location of the rainfall-induced instabilities. For each episode investigated, the ROC curves have been represented (Figure 5c) evaluating two quantities: the False Positive Rate (1-specificity) Eq. (19) and the True Positive Rate (sensitivity) Eq. (20). The diagonal of "random classifier" divides the ROC space. If the point (FPR, TPR) is settled above the random classifier it represents good classification results (better than random) while if it is settled below the line represents bad results (worse than random). ~~It seems reasonable that these extensions are a true representation of the geometry of a shallow landslide so that for each activation detected, 9 pixels have been switched on simultaneously.~~

2.4 Cases sStudied

590 The cases of study considered for calibration and validation of the CRHyME model are located in the Northern Italy (Figure 6): the Caldone the river Caldone catchment (Lecco), Lombardy), and the Valtellina catchment of Adda river in Lombardy, and the Emilia area with the catchments of Trebbia, Nure and Parma rivers across the Emilia areacatchments.

595
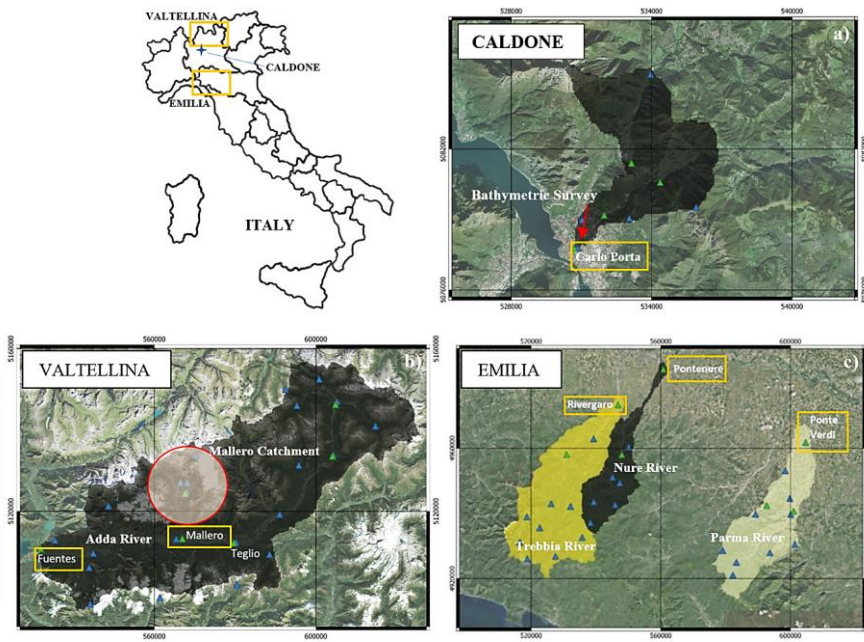
Figure 5: Caldone Rivera a), Valtellina b) and Emilia c) case study. In the red circle is highlighted the Mallero catchment and in orange boxes are the hydrometer stations considered for assessing the CRHyME performances: Carlo Porta for Caldone Catchment, Fuentes and Mallero hydrometers for Valtellina and Rivergaro (Trebbia River), Pontenure (Nure River) and Ponte Verdi (Parma River) for Emilia. Base layer from © Google Maps 2023.

600 • The Caldone basin (Figure 6.a) represents the on-field laboratory of the University of Politecnico di Milano (Brambilla et al., 2020). The basin is about 27 km^2 situated near the city of Lecco (Lombardy) and is characterized by intense sediment transport. The catchment is well monitored by 5 rain gauge stations, a hydrometer at the outlet and two sediment check-dams where the sediment yield is constantly monitored with periodic bathymetric surveys.

The Valtellina valley (Figure 6.b) is comprised of the northern part of the Lombardy region and in 1987 experienced a dramatic 605 geo-hydrological episode triggered by rather intense and prolonged rainfalls. The effects on the territory were severe: shallow

22

landslides, debris flows, and flash floods were recorded causing human injuries and fatalities and extensive damage to infrastructure and buildings (Luino, 2005). Similar events iteratively hit the area also in November 2000 and 2002. The Emilia area (Figure 6.c) experienced intense geo-hydrological episodes respectively in October 2014 and September 2015 (Ciccarese et al., 2020). Three watersheds were particularly affected: river Trebbia, Nure and Parma catchments. The event of October
610 2014 hit the Parma catchment while the event of September 2015 hit the Trebbia and Nure catchments.

Monitoring points were chosen in correspondence with the reference hydrometers located at the catchment outlets (orange boxes in Figures 6a,b,c) for checking the water discharge and volume. Check dams and hHydropower reservoirs were considered for evaluating solid transport. Regarding the shallow landslides and debris flows, a literature survey has been conducted to find an available census of the occurred failures. A pre-simulation of 2 years has been carried out to raise the
615 model to a realistic initial condition (e.g. spin-up period), necessary to achieve the river formation on the valley bottom, the moisturizing of superficial terrain, the recharge of groundwater and a redistribution of the erodible material.

3 Results

3.1 Caldone case study

The Caldone catchment was investigated to assess the numerical conservativity conservativity of CRHyME to hydrological
620 and sediment balance, to explore the sensitivity to the variation of spatial resolution of the input data (e.g. DTM) and to calibrate and validate the slope $-$ D_{50} empirical relations. According to (Rocha et al., 2020; Tavares da Costa et al., 2019), a spatially distributed hydrological model is sensitive to input data resolution. The reconstruction of the catchment parameters, such as the flow accumulation and the flow direction, depends on the characteristic of the DTM. As a result, routing methods may experience differences in results under different cell resolutions since depends on the flow direction. Moreover, increasing
625 the resolution is generally time-consuming due to the large number of cells within the computational domain. To test these aspects in CRHyME, for the Caldone catchment were executed four runs in a short period of 6 months, considering four different DTM resolutions: 90 m, 50 m, 20 m and 5 m. In Table 2 are resumed the simulation settings. To initialize CRHyME, the meteorological data series were gathered from the ARPA Lombardia agency (Rete Monitoraggio ARPA Lombardia) (Figure 6.a). The hydrometers data and the local stage-discharge relation were taken from the Lecco municipality station
630 located at Via Carlo Porta (Figure 76.a). The rain gauges was were spatially interpolated using IDW technique (Chow et al., 1988) with a temporal resolution of 1 day. As can be appreciated from Table 2, the model's ability into the reproduction of a realistic water discharge tends to degrade progressively using a higher resolution. Looking at NSE Q scores, the best accordance with the reference is reached in correspondence of a 50 m resolution. RMSE Q is lower for a 50 m simulation. The model is conservative since NSE V is close to 0.8, verifying that almost all the precipitation volume has arrived at the outlet
635 within the simulated period. NSE V is a parameter that is rather invariant with respect to the resolution.

23

	Simulation 1	Simulation 2	Simulation 3	Simulation 4
Spatial Resolution	90 m	50 m	20 m	5 m
Starting Date	01/05/2020	01/06/2020	01/06/2020	01/06/2020
Ending Date	10/10/2020	10/10/2020	10/10/2020	10/10/2020
Initial Soil Moisture	90%	90%	90%	90%
NSE V [-]	0.765	0.777	0.777	0.656
NSE Q [-]	0.341	0.650	-1.333	-2.610
RMSE Q [$m^3 s^{-1}$]	1.605	0.699	1.804	2.244

Table 2: Setting properties adopted for Caldone River simulations under different spatial resolutions and scoring performances.

	NSE Q	NSE V	RMSE [$m^3 s^{-1}$]
Sediment Transport Simulation	0.462	0.719	0.900

Figure 6: Hydrological simulation carried out for sediment transport assessment: simulated water discharge vs reference hydrometer and hydrological indexes ranking.

The influence of the slope $-$ D_{50} curves parameterization was the second aspect investigated in the Caldone catchment. A long-term simulation has been carried out from 1 January 2019 up to 31 December 2021 (Figure 7), with a DTM resolution of 50 m and after a "spin-up" period of 2 years for rising the model to realistic initial conditions. Considering the limited extension of the watershed, this period has revelated sufficient for assessing the performance of solid discharge. The sediment discharge was computed considering both TL (Transport Limited) and EL (Erosion Limited) options.

24

In Figure 8 7 can appreciate can be noticed that NSE for water discharge (Q) and volume (V) exhibit a rather high score, about 0.462 and 0.719 respectively. The former states that the reproduction of the hydrological part has been assessed almost correctly by CRHyME. Four slope $-$ D_{50} functions have been tested (Table 3): set 1, set 2, set 3 and set 4. Results have shown that the choice of slope $-$ D_{50} can sensibly modify the outlet's sediment yield: the cumulated sediment amount increase with decreasing of in the mean diameter. These data were compared with the onsite bathymetric surveys that were carried out 4 times across the investigated period Table 4. From the bathymetry measurements, a sediment yield of about 1000 m^3 yr^{-1} was considered representative of Caldone River. In our sensitivity analysis, this value has matched the reference using set 2: 2993 m^3 for 1055 days $\approx$ 3 yrs correspond to $\approx$ 1000 m^3 yr^{-1}. Set n° 2 is slightly higher rather than the functions considered for Valtellina and Emilia simulations that are better represented by set n° 3.

Curve Set	a parameter	b parameter	Equations	Total Volume [m^3]
Set 1	5604.8	2.38	$D_{50} = 5604.8\ Slope^{2.38}$	2608
Set 2	1786.9	1.79	$D_{50} = 1786.9\ Slope^{1.79}$	2993
Set 3	1453.1	1.61	$D_{50} = 1453.1\ Slope^{1.61}$	5947
Set 4	285.3	0.8	$D_{50} = 285.3\ Slope^{0.80}$	16446

Table 3 2: Slope $-$ D_{50} functions tested in Caldone catchment and the cumulated volume at the outlet.

Bathymetric survey	Volume
20 July 2019 - 20 July 2020	$\approx 294\ m^3$
20 July 2020 - 13 October 2020	$\approx 438\ m^3$
13 October 2020 - 15 November 2021	$\approx 800\ m^3$

Table 4 3: Bathymetric survey and volume estimation in Caldone River check dam.

3.1 2 Valtellina c Case s Study

The analysis conducted for the Valtellina area has followed the steps reported in Table 2 5. The CRHyME calibration for Valtellina was carried out for three years comprised between 1 September 2015 and 31 August 2018 after a "spin-up" period of 2 years for realistic initial conditions. Then, a subsequent validation period started on 1 September 2018 up to 31 December 2019. In Figure 9 the water discharges and the total volumes computed by CRHyME in the two reference sections of Fuentes (basin area = 2600 km^2) and Mallero (basin area = 320 km^2) are reported. Two different meteorological datasets were examined here to test the ability of CRHyME to deal with different input data. The first one has considered the meteorological data provided by the Regional Agencies for Environmental Protection (ARPA Lombardia) (Rete Monitoraggio ARPA Lombardia) ground-based weather stations. The second one is MERIDA, the MEteorological Reanalysis Italian Dataset (Bonanno et al., 2019). MERIDA consists of a dynamical downscaling of the new European Centre for Medium-range Weather Forecasts

(ECMWF) global reanalysis ERA5 using the Weather Research and Forecasting (WRF) model, which is configured to describe the typical weather conditions of Italy.

675 ~~Simulation settings of Valtellina case study. The first calibration and validation of the model have considered more than 4 years of data on daily basis gathered from ARPA (Environmental Agency) (Rete Monitoraggio ARPA Lombardia) weather stations and the MERIDA reanalysis database (Bonanno et al., 2019). These event-based simulations were carried out for significant geo-hydrological events of July 1987, November 2000 and November 2002.~~

Valtellina catchment	Starting Date	Ending Date	Rainfall Dataset used
Calibration	01/09/2015	31/08/2018	ARPA Lombardia and MERIDA
Validation	01/09/2018	31/12/2019	ARPA Lombardia and MERIDA
1987 event	01/09/1984	31/07/1987	ARPA Lombardia
2000 event	01/09/1997	30/11/2000	ARPA Lombardia
2002 event	01/12/2000	31/12/2002	ARPA Lombardia

680 **Table 5: Simulation settings of Valtellina case study. The calibration and validation of the model have considered more than 4 years of data on a daily basis gathered from ARPA (Environmental Agency) (Rete Monitoraggio ARPA Lombardia) weather stations and the MERIDA reanalysis database (Bonanno et al., 2019). These event-based simulations were carried out for significant geo-hydrological events of July 1987, November 2000 and November 2002.** ~~Table 2: Simulation settings of Valtellina case study. The first~~
685 ~~calibration and validation of the model have considered more than 4 years of data on daily basis gathered from ARPA (Environmental Agency) (Rete Monitoraggio ARPA Lombardia) weather stations and the MERIDA reanalysis database (Bonanno et al., 2019). These event-based simulations were carried out for significant geo-hydrological events of July 1987, November 2000 and November 2002.~~

Simulation 2015-2019	NSE [-]	RMSE [mm m³ s⁻¹]	NSE_MERIDA [-]	RMSE_MERIDA [mm m³ s⁻¹]
Q Fuentes	0.199	45.370	-0.603	64.172
V Fuentes	0.783	1.587 10⁹	0.993	2.931 10⁸
Q Mallero	0.325	4.695	-2.369	10.494
V Mallero	0.988	2.852 10⁷	-0.145	2.736 10⁸

Figure 7: CRHyME model simulation results of water discharges (left) and volume (right) at Fuentes (a), and Mallero (b) hydrometers for the period 2015-2019 and using ARPA weather stations and MERIDA dataset. As can be appreciated, the Volume performances are better that Discharge performances: the Valtellina basin is strongly regulated by hydropower plants and dams that operate a consistent lamination of the peak discharge during major rainfall events; the kinematic routing may be not sufficiently accurate for flood propagation across the valley floodplain since dynamic lamination may occur. As a result, green and blue spikes overestimate the peak discharge with respect to the reference.

c) Curve Set	*a* parameter	*b* parameter	Empirical Equations	Reference
Set 1	5604.8	2.38	$D_{50} = 5604.8\ Slope^{2.38}$	From (Berg, 1995), b = 2.38
Set 2	1786.9	1.79	$D_{50} = 1786.9\ Slope^{1.79}$	Decreasing a and b
Set 3	1453.1	1.61	$D_{50} = 1453.1\ Slope^{1.61}$	Decreasing a and b

Set 4	285.3	0.8	$D_{50} = 285.3\ Slope^{0.80}$	Decreasing a
Set 5	246.7	0.8	$D_{50} = 246.7\ Slope^{0.80}$	Decreasing a
Set 6	142.6	0.8	$D_{50} = 142.6\ Slope^{0.80}$	From (Nino, 2002), b = 0.8
Set 7	95.1	0.8	$D_{50} = 95.1\ Slope^{0.80}$	Decreasing a

d)

Sediment Yield	Campo Tartano Dam	Valgrosina Dam	Cancano Dam
Reference	38'037 m^3/yr^{-1}	33'600 m^3/yr^{-1}	21'450 m^3/yr^{-1}
Simulated 2015-2019	33'604 m^3/yr^{-1}	34'324 m^3/yr^{-1}	18'893 m^3/yr^{-1}
%	-11.7 %	+2.15 %	-11.9 %

Figure 8: a) Valtellina case study area where blue triangles represent rain gauge stations while red triangles are hydropower reservoirs; b) and c) $Slope - D_{50}$ relations tested and implemented in CRHyME based on the theory of (Berg, 1995; Nino, 2002) and considering on-site surveys; d) Sediment yield estimations for three dams of Campo Tartano, Valgrosina and Cancano (orange boxes) where can be noticed the correct estimation with respect to the ITCOLD reference (ITCOLD, 2009, 2016). Base layer from © Google Maps 2023.

Looking at the simulation driven by the ARPA dataset, the total volume transited at the Fuentes section (line blue, Figure 8.a) is underestimated if compared to the local hydrometer reference (line red), while at the Mallero section (line blue, Figure 8.b) simulated and recorded volumes are in agreement. Also, NSE scores for volumes highlight this fact since Mallero's NSE ~1 while Fuentes's NSE is about 0.783, significantly lower. Transited volume is the integral of water discharge that CRHyME has better reproduced for the Mallero section (agreement among blu and red line in Figure 8.b and NSE = 0.325) rather than Fuentes's section (disagreement among blu and red line with underestimation of the mean flow during minter periods in Figure 8.b and NSE = 0.199).

Opposite results were obtained considering MERIDA's dataset. There, the Fuentes section has performed well both in discharge and volume computation rather than the Mallero section. Volume NSE at Fuentes is now closer to the perfect agreement while at Mallero station the transited volume is strongly overestimated. In both cases, NSE scores for discharges are badly represented with values below the '0' threshold. This fact is also well depicted in Figure 8 where discharge spikes simulated from the ARPA dataset (blue line) are lower with respect to the green ones simulated from the MERIDA dataset. The CRHyME model performed numerically conservatively in both cases without code instabilities so that these outcomes are supposed to be perturbed by the different reconstructions of rainfall fields. From these results can be noticed how the influence of rainfall data is determinant in the hydrological assessment. Looking at RMSE scores, the simulation with the ARPA dataset has better performed giving lower values of the index, around 4.7 m^3 s^{-1} and 45.4 m^3 s^{-1} for Mallero and Fuentes sections respectively. This means that discharge uncertainties propagate proportionally increasing the extension of the catchment and CRHyME's performances are sensibly higher for small catchments.

Sediment transport results were checked in correspondence with three hydropower reservoirs of Campo Tartano, Valgrosina and Cancano (Figure 9.a) considering ARPA dataset simulations. For each reservoir, a literature survey has been conducted to estimate the yearly mean sediment accumulation (Ballio et al., 2010; Milanesi et al., 2015; ITCOLD, 2016).

The sensitivity parameter for sediment yield is represented by the slope $-$ D_{50} curve that was adjusted during the calibration period (Figure 9.b and 9.c). ~~Since it doesn't exist a close formulation for indirectly estimating the granulometry in absence of a field survey dataset different functions have been proposed taking into account literature surveys and approaches proposed by (Nino, 2002; Sambrook Smith and Ferguson, 1995; Lamb and Venditti, 2016; Berg, 1995). Several Slope $-$ D_{50} relations were retrieved from the studies and obtained varying the parameters of the curves. These relations mimic the functions proposed by (Berg, 1995) where the D_{50} is determined as a function of the river morphology evolution, varying the two power-law coefficients.~~ Among others, the set n°6 was retained sufficiently representative ~~for~~ of the Valtellina area. In Figure 9.d is reassumed the results obtained from CRHyME simulations where the sediment yields evaluated on a yearly based have matched the reference data for the three reservoirs investigated. For the Campo Tartano dam, the difference between the simulated and the reference is around -11.7%, for the Valgrosina dam is about +2.15% while for the Cancano reservoir is around -11.9%.

The capacity of CRHyME in predicting the localization of shallow landslides triggered during the events of 1987, 2000 and 2002 events was investigated through the ROC scores. Figure 10 describes the ROC assessment for the shallow landslides that occurred in Valtellina during the July 1987, November 2000 and November 2002 events. T~~a compar~~he four ~~shallow~~ landslide instability models included in CRHyME (Iverson, Harp, Milledge, and SLIP) ~~has been carried out~~were compared, ranking the Harp model as the most accurate one. A realistic combination of friction angle values ~~has been~~was considered ~~for the area~~: 40° for gravels, 35° for sand, 33° for silt and 30° for clay. In analogy with root cohesion, ~~To obtain a spatial distribution of t~~the friction angle was spatially distributed ~~, this combination has been weighted~~ by considering the ~~fraction of~~ soil composition (%coarse, %sand, %silt, %clay) within the superficial layers ~~retrieved directly~~ (Hengl et al., 2017)~~from available soil data~~. Using the Harp model ~~and considering different buffer extensions of 250 m, 500 m, 1000 m and 2000 m. Among others, the Harp model has performed best with respect to the others, followed in the order by Milledge, Iverson and SLIP models. In Figure 11 are reported the results obtained by Harp model varying the buffer extension around the census landslide point.~~ for the three event~~s case~~, the ROC curves have ~~assessed~~ranked ~~a model~~CRHyME's performance above the "random classifier" threshold line. The sensitivity (True Positive Rate) of the model is generally comprised of between 0.2 and 0.6 while the 1-specificity (False Positive Rate) is around 0.2. The distorted distribution of the shallow landslide census related to 1987 may have influenced the performance predictions, lowering the ROC assessment with respect to the events that happened in 2000 and 2002 events. The buffer's choice ~~of the buffer extension~~ can influence the redistribution among TP and FP: ~~and generally,~~ the performance ~~may tend to~~is lower when large buffers are considered, especially for 1000 m and 2000 m radii which tend to increase with ~~. On the other hand,~~ the radius of 250 m and 500 m ~~are~~closest to the actual extension of shallow landslide ~~movements~~recorded.
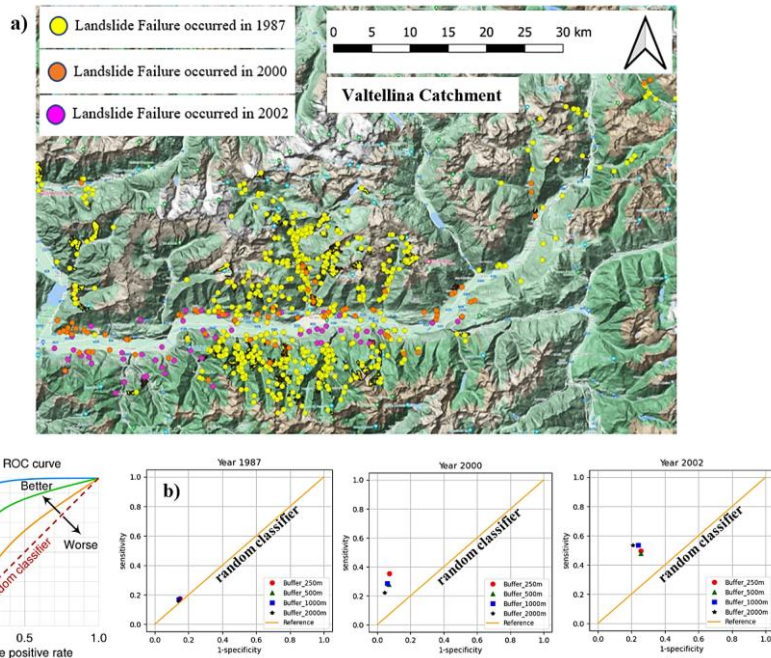
Figure 9: a) Triggered shallow landslides during the events of July 1987 (yellow points), November 2000 (orange points) and November 2002 (fuchsia points) across the Valtellina area from IFFI. b) ROC curves for 1987, 2000 and 2002 events considering the model Harp. Base layer from © Google Maps 2023. ~~For the examined case studies, the model has shown a good ability to correctly individuate the location of the triggered landslide.~~

~~In every case, the ROC curves have assessed a model performance above the "random classifier" threshold line. The sensitivity (True Positive Rate) of the model is generally comprised of between 0.2 and 0.6 while the 1-specificity (False Positive Rate) is around 0.2. The distorted distribution of the shallow landslide census related to 1987 may have influenced the performance predictions, lowering the ROC assessment with respect to 2000 and 2002 events. The choice of the buffer extension can influence the redistribution among TP and FP and generally, the performance may tend to lower when large buffers are considered, especially for 1000 m and 2000 m radii. On the other hand, the radius of 250 m and 500 m are closest to the actual extension of shallow landslide movements. For the examined case studies, the model has shown a good ability to correctly individuate the location of the triggered landslide.~~
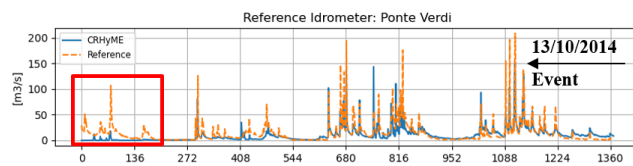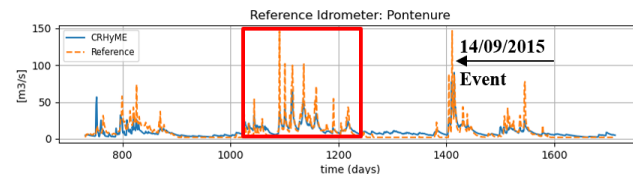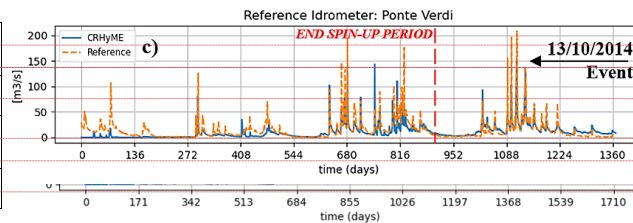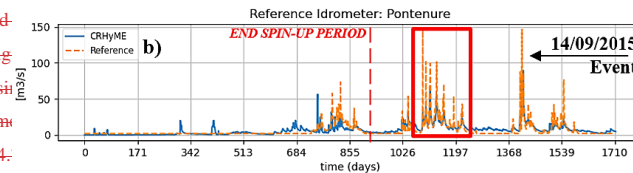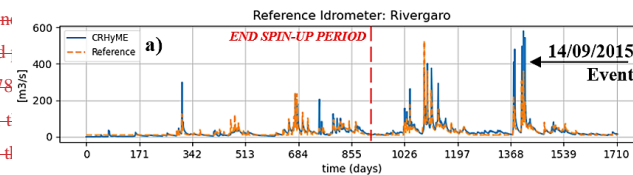
3.1 3 Emilia cCase sStudy

770 For the Emilia case study, CRHyME was tested following a similar schedule for the Valtellina area. Simulations were carried out considering a period of 5 years from 01/09/2011 up to 31/12/2015 where geo-hydrological events of 13/10/2014 and 14/09/2015 have been recorded in the area (Table 36). To raise the model to a realistic initial condition, a spin-up period of 900 days comprised between 01/09/2011 and 28/02/2014 have has been consideredcarried out. ARPA Emilia meteorological dataset (Rete Monitoraggio ARPA Emilia) was considered for rainfall and temperature variables.

775

Emilia's catchments	Starting Date	Ending Spin-Up Period	Ending Date	Rainfall Dataset used
River Trebbia	01/09/2011	28/02/2014	31/12/2015	ARPA Emilia
River Nure	01/09/2011	28/02/2014	31/12/2015	ARPA Emilia
River Parma	01/09/2011	28/02/2014	31/12/2015	ARPA Emilia

Table 6: Simulation settings of Emilia case study considering the ARPA Emilia **(Rete Monitoraggio ARPA Emilia)**.Table 5: Simulation settings of Emilia case study considering the ARPA Emilia (Rete Monitoraggio ARPA Emilia)

After running CRHyME for the entire simulation period, keeping the calibration parameters assessed for the Valtellina case
780 study, the model scores have been examin~~ed~~
water discharge reproduction for the tested
water volume especially for Nure (0.978
However, with respect to Valtellina area, t~~he~~
rivers (0.452) while for Nure t~~he~~
785 Looking at the solid transport quantificatio~~n~~
del Fiume Po, 2022) estimations obtained
AdBPo data were calculated by applying
Valtellina, the results obtained after the si~~mulation~~
cases, the order of magnitude of the sedim~~ent~~
790 Trebbia (+12.6%) and Parma (24.

Hydrology Vars.	NSE [-]	RMSE [m³ s⁻¹]
Q Rivergaro	0.272	27.915
V Rivergaro	0.773	5.450 10⁸
Q Pontenure	0.102	33.468

V Pontenure	0.978	~~3.765 10^7~~
Q Ponte Verdi	0.452	14.898
V Ponte Verdi	0.482~~0~~	~~3.704 10^8~~

Sediment Yield	Trebbia River
AdbPo Reference	$247.2\ 10^3\ m^3\ yr^{-1}$
Simulated	$278.3\ 10^3\ m^3\ yr^{-1}$
%	+12.6 %
Nure River	Parma River
$69.4\ 10^3\ m^3\ yr^{-1}$ ~~/yr~~	$101.1\ 10^3\ m^3\ yr^{-1}$
$44.6\ 10^3\ m^3\ yr^{-1}$ ~~/yr~~	$76.1\ 10^3\ m^3\ yr^{-1}$
-35.7 %	-24.7 %

Figure 10: CRHyME model simulation results of water discharges, liquid volume, solid discharge, and solid volume at a) Rivergaro (Trebbia River), b) Pontenure (Nure River), c) Ponte Verdi (Parma River) for the period 2011-2015. The first 900 days of each simulation are considered for model "spin-up" to a realistic initial condition. In the red box ~~are~~ is highlighted the peak discharge overestimation for Nure river.

~~up to~~The hydrology of the Trebbia, Nure and Parma rivers has shown similar scores to the Valtellina area. Looking at NSE, we can appreciate that higher scores are assessed for the water volume of Nure River (0.978), Parma River (0.820) and Trebbia River (0.773). For water discharges, NSE scores are better for Trebbia (0.272) and Parma rivers (0.452) while for Nure River are lower (0.102), also confirmed by the RMSE index (Figure 11).

Looking at the solid transport quantification, the AdBPo (Autorità di Bacino del fiume Po) reports have been~~were~~ taken into consideration as reference data for the comparisons (Autorità di Bacino Distrettuale del Fiume Po, 2022). Keeping the same calibration of the $slope - D_{50}$ curve (set n°6) that was adopted for the Valtellina, the results obtained after the simulations have shown fairly good accordance with the reference. In the three cases, the order of magnitude of the sediment yield delivered each year at the outlet is similar to AdBPo data especially for Trebbia (+12.6%) and Parma (-24.7%) basins while for Nure we have a slightly larger difference (-35.7%). This suggests how the sediment transport dynamics are sensitive to the $slope - D_{50}$ parameterization that strongly depends on the geological characteristics of the catchment.

The performance of CRHyME in detecting the triggered debris flow during the events of October 2014 and September 2015 (Figure ~~11~~12) was assessed again through ROC methodology. A brief sensitivity analysis on the value of the friction angle was carried out since the value provided for the Valtellina was too conservative ~~with respect to~~for stability. The highest ROC scores were obtained by slightly decreasing (20%) the slope friction angles and reducing the soil cohesion to the minimum,

32

supposed to be representative of incoherent deposits. In most cases the model has outperformed the random classifier, showing a sensitivity (TPR) comprised between 0.1- 0.4 and a higher value of specificity (1-FPR) depending on the chosen buffer extension around the triggering point. In our simulations, debris flow failure has been effectively detected across a small valley impluvium confirming the onsite observations carried out by (Ciccarese et al., 2020; G. et al., 2021).
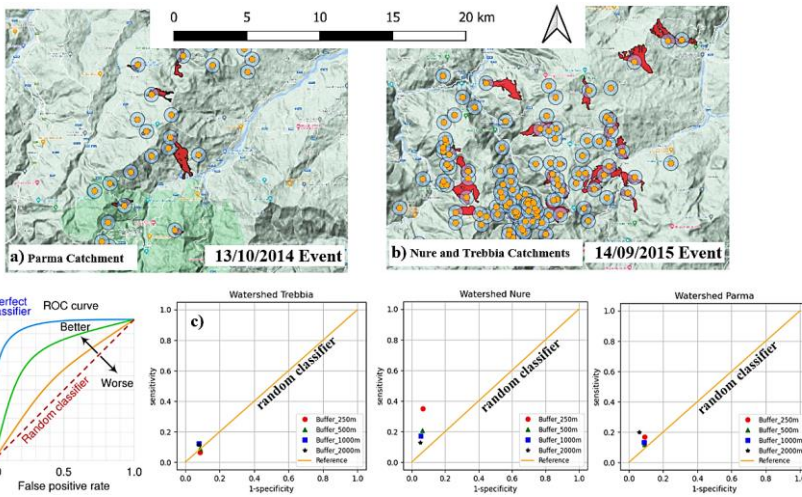
Figure 11: ~~a) Trebbia-Nure landslide triggered during the event of September 2015 (left)~~ a, b) **Debri flows triggered in Parma basin during the event of October 2014 (**~~right~~left**), b) Debris flows** triggered **in Trebbia and Nure basins** during the event of September 2015 (right)**. Orange points are the mass wasting starting points, blue circles represent a buffer around the point and red polygons are the IFFI landslide census mapped in the area and c) ROC curves for Trebbia, Nure and Parma watersheds for the debris flow events of October 2014 and September 2015. Base layer from © Google Maps 2023.**

4 Discussion

4.1 CRHyME sensitivity analysis: spatial resolution and sediment diameters

The sensitivity of the CRHyME model has been tested for four different spatial resolutions within the Caldone catchment (27 km²): 90 m, 50 m, 20 m and 5 m. CRHyME results were obtained with sufficient accuracy and faster computation for cell resolution > 10 m. In fact, the computational time was observed to be proportional to the number of domain cells: the 90 m, 50 m and 20 m simulations were concluded in one-two minutes while for the 5 m simulation, the time has increased up to 5 min. However, increasing spatial resolution doesn't mean always increasing the accuracy (Rocha et al., 2020; Zhang et al., 2016) and with CRHyME the best performance was acquired for spatial resolutions of 50 m and 20 m and not for 5 m. In fact, the variation of the DTM resolution can change sensibly the flow direction of the rivers ("ldd.map") and the basin drainage

33

density affecting discharge computation. Moreover, according to the literature (López Vicente et al., 2014; Erskine et al., 2006), the routed runoff could be perturbed by "numerical diffusion", a known problem of the spatially distributed models that is predominant with fine spatial resolution, that depends on the algorithm applied for flow direction computation (Barnes, 2017, 2016). To preserve CRHyME's solution accuracy and to maintain affordable computational times, we suggest applying the HydroSHED DTM model at 90 m resolution for quite-large basins > 500 km^2 while higher resolutions are advisable for smaller basins.

Within the Caldone catchment, the dependence of the sediment transport processes on the soil granulometry was tested. The distribution of D_{50} that increase as a function of the slope is a reasonable representation of the geomorphological processes that can be encountered in mountain catchments (Brambilla et al., 2020; Ivanov et al., 2020a; Ballio et al., 2010). According to (Nino, 2002), among slope and D_{50} exist a slight correlation, but non-linearities are caused by sediment processes occurring within rivers granulometry (sorting and armouring). Recently, data-driven approaches were explored in the USA for defining a map of the D_{50} along the river stream (Abeshu et al., 2021). To evaluate the map, these authors have chosen a series of geo-morphological predictors of D_{50} such as slope, elevation etc. verifying results with the available databases at country-based they have retrieved the USA D_{50} map. Not surprisingly, one of the most important predictors is the basin slope which has the highest correlation coefficient with a D_{50}. However, the authors stated that other geomorphological factors (river path length and elevation) have a similar correlation with D_{50}. It seems clear that a unique formulation of the D_{50} as a function of morphological and hydrodynamical parameters cannot be assessed straightforwardly. Since D_{50} is required for incipient motion of bed-load sediment transport (Chow et al., 1988), and bearing in mind its complexity in spatial evaluation, slope − D_{50} curves implemented in CRHyME represent a crude but efficacious simplification. Moreover, slope − D_{50} have the advantages to be easily calibrated in the function of available data on-site.

4.2 CRHyME's hydrological performances

For the Valtellina case study, CRHyME hydrological performances looking at the water discharge (NSE ~ 0.2-0.3) were not comparable with respect to the river Caldone (NSE ~ 0.46). A possible explanation resides within the characteristics of the Valtellina catchment, which is bigger (2600 km^2) than the Caldone basin (27 km^2).

Bigger computation domains mean increased landscape heterogeneity which implies higher uncertainties in the reproduction of infiltration-runoff-groundwater processes (Morbidelli et al., 2018; Mishra et al., 2003; Chow et al., 1988). Comparing volume and discharge scores for the Valtellina area driven by the ARPA dataset, a general tendency to overestimate the peak discharge during rainfall seasons (spring, summer and autumn) can be noticed while an underestimation of the discharges during winter is detected (Figure 9.a). This effect is more significant at Fuentes hydrometer but is less evident at Mallero station. After analysing these discharge results, three main error components were disentangled into 1) infiltration, 2) losses, and 3) routing parameterizations. They represent key processes which should be paid attention to during the calibration phase (Morbidelli et al., 2018) since if they are wrong-conditioned may also cause numerical instabilities, losing the conservativity of the code. As reported by (Abbate and Mancusi, 2021a), infiltration models strongly regulate runoff generation. Their

34

parameterization depends on land surface coverage and terrain composition which are sometimes affected by high uncertainties since onsite measurements are generally not available. For CRHyME, this fact may imply cascade effects on landslide processes causing underestimation of the landslides triggered due to the reduced subsurface pore pressure caused by wrong soil moisture balance predictions. Water recirculation inside the groundwater reservoir generally affects water balance in the long term. In this regard, Alps and Apennines have complex hydrogeology (ISPRA, 2018) which affects the groundwater dynamics that a simple Dupuit model may oversimplify. Unfortunately, the unavailability of local piezometric reference data for calibration has not permitted us to assess model performance for this part. To cope with these uncertainties, several sensitivity tests (not reported) were conducted varying groundwater parameterization to achieve the best performances. Another source of error is embedded within the runoff-routing algorithm. The kinematic runoff-routing model adopted in CRHyME is sufficiently representative of the small lateral catchment rainfall-runoff processes (as for Caldone or Mallero rivers) but maybe not be suitable for interpreting floodplain flood evolution where dynamic processes are prevalent (Chow et al., 1988). Moreover, across the Valtellina catchment, river discharges are regulated by several hydropower plants (ITCOLD, 2009, 2016). Dams can smooth and shift floods peaks and perturb seasonal water discharges recorded at the outlet's hydrometer lowering the CRHyME performances since in the current version of the model lakes and dams are not considered explicitly. Among others, this fact could explain the best score (NSE = 0.325) of the Mallero sub-catchment (less regulated, only 2 dams) with respect to the Fuentes outlet (NSE = 0.199) for the whole Valtellina catchment (Figure 6).

The hydrological performances of Emilia catchments have scores similar to the Mallero River. The water discharge assessment for the tested period shows the best agreement for Trebbia (NSE ~ 0.27) and Parma (NSE ~ 0.45). These basins are less regulated by hydropower reservoirs with respect to the Valtellina, and, since they are smaller (about 1/3 of the extension), the kinematic approach for runoff routing is more representative. Nevertheless, the lower scores for the Nure River are caused by an overestimation of the peak discharges (Figure 11). Several simulations conducted in the Nure basin have shown a systematic bias within the reference data. The latter could be explained by the location of the reference hydrometer which is settled far away across the flood plain, experimenting a peak lamination. Looking at Figure 5, the Pontenure hydrometer is located across the flood plain ~20 km downstream of the catchment for the Rivergaro (~1 km) and Ponte Verdi (~10 km) stations. Similar to Valtellina, a flood lamination is likely to occur before reaching the stations so a dynamic approach should be tested instead of kinematic routing to increase the discharge agreements.

4.3 CRHyME's geo-hydrological performances

Geo-hydrological processes have been physically consistently reproduced by CRHyME. The sediment yields calculated on a yearly based have been matched for the available reference data of Tartano, Valgrosina and Cancano dams after a calibration of the slope - D_{50} to distribute grain size parameters across the catchment. The good reproduction of the annual sediment yield (~ 10% underestimation for Valtellina) has been confirmed also for the Emilia case study where the order of magnitude was correctly reproduced with respect to AdBPo reference (± 20% depending on the basin).

35

Since the D_{50} perturbs the threshold that activates the sediment transport (Vetsch et al., 2018), it has revealed the critical parameter to be assessed in the CRHyME model. For Valtellina and Emilia areas, the optimal $slope - D_{50}$ curve was rather different with respect to the one adopted for the Caldone catchment. From a geological viewpoint, the Caldone catchment is in the pre-alps where calcareous rocks are prevalent with respect to Valtellina and Emilia where metamorphic bedrock is more diffused (ISPRA, 2018). Depending on the state of fracture, metamorphic could be less strength than calcareous and more prone to be fragmented into small diameters (D'Agostino and Marchi, 2001). Moreover, also the maturity of the watershed influences the granulometry distribution across the landscape (Pérez-Peña et al., 2009; Strahler, 1952). Large basins such as Valtellina and Emilia catchments are undoubtedly more "mature" than the small Caldone catchment, therefore, a finer granulometry at the outlet is expected. This fact seems to justify why a lower $slope - D_{50}$ curve was optimal for these catchments while a higher one was more suitable for the Caldone basin.

The CRHyME model has identified the localization and the timing of landslide failures during the extreme events that have affected the studied catchment. Looking at ROC scores for the Valtellina area, 1987, 2000 and 2002 events were reproduced consistently. The best scores were acquired for 2000 and 2002 events also a good quality census was available for the investigated area. For 1987, as can be appreciated in Figure 10, the incompleteness of the available census (yellow points) has affected the model's final score. However, independently from the specific case, the ROC methodology has highlighted how much the choice of stability parameters (friction angle and cohesion) has a critical influence on the final results. This fact has been confirmed also by the sensitivity analysis carried out for debris flow episodes in the Emilia case study during the event of 2014 and 2015. Here, to reach the best ROC scores with respect to the random classifier, the friction angles calibrated for Valtellina have been slightly reduced by about 20%.

4.4 Model limitations

The main model limitations encountered during CRHyME's tests regard three aspects: precipitation mapping, initial conditions settings and geo-hydrological cycle parametrization. Correctly assessing the precipitation distribution is mandatory to define a realistic representation of the external forcing that triggers geo-hydrological failures (Abbate et al., 2021b). Especially across mountain regions, the higher local variability of meteorology and the absence of a dense rain gauge network can complicate the reconstruction of a representative rainfall field. This aspect was investigated for the Valtellina case study, where simulations derived by MERIDA (Bonanno et al., 2019) and ARPA (Rete Monitoraggio ARPA Lombardia) datasets were compared. Using MERIDA, we would expect a better performance from CRHyME runs but this didn't happen in all situations. Looking at water volumes transited across the Fuentes hydrometer during the period 2015-2019, the MERIDA dataset has performed better than ARPA stations. On the other hand, looking at the Mallero hydrometer, the MERIDA dataset has scored worse than ARPA stations. What is the possible explanation for this contradictory fact? MERIDA gives a rainfall map that has a spatial resolution of 4 km while the ARPA stations data are interpolated geometrically using the Inverse Distance Weight (IDW) techniques (Daly et al., 1997; Chow et al., 1988). A trade-off exists between the ARPA's rain gauge network density and the spatial resolution of MERIDA. In large catchments, MERIDA is more representative since it can cover ungauged areas while in small

36

catchments, lower spatial resolution may be insufficient for describing local rainfall. This is why MERIDA has performed worse rather than IDW in the Mallero catchment where several ground-based weather stations are uniformly distributed across a limited area of 320 km^2. Moreover, reanalysis datasets could sometimes smooth the rainfall peaks leading to a wrong interpretation of the net rainfall that occurred over a limited area (Abbate et al., 2021b; Bonanno et al., 2019; Ly et al., 2013).

935 This is another key issue that generally influences the ability of the slope stability model to detect landslides triggered by rainfalls. In this regard, a better integration within rainfall sources coming from the ground-based station, reanalysis models, radars maps and satellite data is advisable to reduce possible rainfall uncertainties (Abbate et al., 2021b).

The choice of a realistic initial catchment's moisturizing is another common issue in every deterministic spatially-distributed hydrological model (Uber et al., 2018; Tramblay et al., 2010; Chow et al., 1988). It is very difficult to have sufficient historical

940 measures about the superficial soil moisture, groundwater piezometry and superficial runoff, especially across small basins. Moreover, soil moisture is a quantity that can vary abruptly across different terrain types, so it is not common to implement a network that permits the acquisition of distributed information across a catchment (Lazzari et al., 2018). In CRHyME, to overcome these difficulties, a "spin-up period" was introduced within each simulation. This period represents the minimum time required by the model for reaching an automatic adjustment of the initial condition that depending on the extension of the

945 basin, can be comprised within a few months up to some years. In fact, the spin-up simulation permits a re-distribution of the water across the cells of the domain (horizontally) and among each layer of the model (vertically), reducing the "time lag" between rapid (runoff) and slow (groundwater) catchment dynamics. This "time lag" effect was rather evident for the Emilia case study, where a realistic regime condition was reached only after three of years, rather slower than for the Adda basin (2 years). This fact could be explained by the different soil compositions that influence hydrogeological parameters. In the

950 Apennines, the presence of clay decreases the speed of soil recharge (lower permeability) slowing down the groundwater recharge (Ronchetti et al., 2009; Ciccarese et al., 2020) with respect to the Alps, where coarser terrain granulometry increases soil permeabilities. From a practical viewpoint, running the model up to realistic hydrological conditions is time-consuming. In CRHyME, PCRaster libraries are already parallelized and can reduce sensibly the computational cost of this operation. Moreover, CRHyME can set a "restart" condition, saving the "main state" outputs of hydrological storage quantities

955 $\Delta h_{snow}(t)$, $\Delta h_{soilwater}(t)$, $\Delta h_{groundwater}(t)$ and $\Delta h_{runoff}(t)$ computed during the spin-up period which could be reused for subsequent running.

According to (Gariano and Guzzetti, 2016), reconstructing the whole geo-hydrological cycle that drives the erosion and mass wasting processes through numerical models is a challenge. In this regard, CRHyME is not an exception: EPM is considered for erosion; empirical power-law relationships are implemented for sediment routing; only landslide and debris flow triggering

960 conditions are evaluated by stability models, not including runout evolutions. This subdivision was adopted firstly to simplify the phenomena interactions and secondly for guaranteeing the fast functioning and stability of the CRHyME code. Following this sequential scheme, geo-hydrological processes are computed after the hydrological assessment, but feedbacks are not explicitly taken into account. On a long-term timescale, geo-hydrological processes contribute to a landscape modification, e.g. DTM's height changes. The former is not contemplated by CRHyME since the code has been built with a different purpose

37

with respect to landscape-evolutions models (Campforts et al., 2020; Bovy et al., 2020; Salles, 2019). However, all geo-hydrological hazards play an important role also on short-term modifying temporarily or permanently the local soil depth (Sklar et al., 2017): landslide and debris flow runout can redistribute the local terrain changing the soil depth (asportation at the crown and accumulation at the toe) and modifying the DTM height. Therefore, finding a "closure" for the "superficial geo-hydrological balance" is a non-trivial task from a theoretical and numerical viewpoint. In fact, the CRHyME experience has shown how landslides and debris flow stability assessment cannot be treated deterministically since their triggering depends on the friction angle of the natural slope, and the cohesion of the superficial soil which are unknown parameters. (Abbate and Mancusi, 2021a)Following some literature studies (Hengl et al., 2017; Yu et al., 2018; Dade and Friend, 1998b; Chow et al., 1988) cohesion was spatially distributed in the function of vegetation coverage bearing in mind the roots contribute to stability while the friction angle was correlated with the soil composition. On the other side, friction angle is in function of soil consolidation which is barely unknown, depending also on complex sediment dynamics and geological processes (de Vente and Poesen, 2005; Merritt et al., 2003; Shobe et al., 2017; Ballio et al., 2010; Kondolf, 1997). Unfortunately, the tuning procedure within a sensitivity analysis was necessary case-by-case since these parameters do not have strong geo-morphological predictors to be correlated on. The assessment of the "superficial geo-hydrological cycle" cannot be evaluated precisely since its monitoring is currently still insufficient on a catchment scale (ISPRA, 2018). Even though surface mapping and census are supposed to increase their accuracy and completeness in the future, some doubts remain about possible improvements for other fundamental data required for physically based slope stability models. In this sense, the databases adopted in CRHyME (Hengl et al., 2017; Huscroft et al., 2018; Ross et al., 2018) have already made an important homogenization of the essential data required for geo-hydrological modelling.

4 (Barnes, 2017, 2016)(Albano et al., 2017; Brunner et al., 2015; Hunter et al., 2008)(Barnes, 2016)(ISPRA, 2018)(Dade and Friend, 1998b)(Abeshu et al., 2021)

4.1 The hydrological performance of Valtellina and Emilia case studies

As shown in the previous paragraph, CRHyME hydrological performances are not particularly satisfactory regarding the water discharge reproduction (NSE ~ 0.2-0.3), especially for the case study of Valtellina considering both ARPA and MERIDA datasets. The characteristics of Valtellina catchments, where river discharges are regulated by the presence of a consistent group of hydropower plants (ITCOLD, 2009, 2016) can decrease the CRHyME performances in reconstructing the water discharges peaks recorded at the outlet. In fact, in the current version of the model lakes and dams are not considered since still data about how they operate and flood regulations are not available to the public. On the other hand, the kinematic routing of runoff, which is sufficiently representative of the small lateral catchment rainfall-runoff processes (Chow et al., 1988), maybe not be suitable for interpreting floodplain flood evolution where dynamic routing should be considered. In fact, due to its morphology, Valtellina valley has a rather long floodplain (70 ~ 80 km) where larger river sections are present together with 4 in-line reservoirs that can operate important flood lamination during intense rainfall events. This explains the best score

38

of the Mallero sub-catchment (NSE = 0.325) with respect to the Fuentes section (NSE = 0.199) related to whole Adda catchment.

As a counter-example, the hydrology of Emilia rivers has similar scores of Mallero in water discharge reproduction for the tested period with the best agreement for Trebbia (NSE ~ 0.27) and Parma (NSE ~ 0.45). These basins are less regulated by hydropower reservoirs with respect to the whole Valtellina, and, since they are smaller (about 1/3), also the kinematic approach for runoff routing is much more representative of the catchment behaviour. Nevertheless, for the Nure river, the lower scores are caused by the appreciable differences between CRHyME discharge peaks that overestimate during rainfall periods the ones recorded by the hydrometer, even though the catchment behaviour seems to be represented correctly thanks to the volume conservation (NSE ~ 0.978). Looking at Figure 5, Pontenure hydrometer is located across the flood plain ~20 km downstream of the catchment with respect to the Rivergaro (~1 km) and Ponte Verdi (~10 km) stations. Similar to Valtellina, a flood lamination is likely to occur before reaching the stations so a dynamic approach should be tested instead of kinematic routing in order to increase the discharge agreements.

The higher performances in the volume quantification obtained by CRHyME in almost all tested cases (NSE ~ 0.8-0.9) assure that the routine is numerically and hydrologically conservative. Numerical stability has been guaranteed by built-in PCRaster libraries adopted for computations where some stability criteria have been matched especially for kinematic and dynamic routing functions. Since hydrological balance and water redistribution across the catchment domain are rather articulated, CRHyME calculates the ratio among the water Inflows and Outflows at each time step: if the model works numerically conservatively it is kept equal to 1. The high value of the NSE index has shown that the behaviour of the catchment dynamic over a long period of simulation is correctly interpreted. This is true especially for the Valtellina case study, using the ARPA dataset, and for Trebbia and Nure basins while only for Parma the score was sensible lower. A possible explanation may reside in some errors that affected the early simulation period where the CRHyME model has not already reached the regime condition giving a non-optimal reconstruction of the water discharge.

Comparing volume and discharge scores a general tendency to overestimation of the peak discharge during rainfall seasons can be noticed while an underestimation of the discharges during winter is detected. The main reason should be imputed also in part to the water recirculation inside the groundwater reservoir that, as already anticipated in section 2, has been included bearing in mind several assumptions due to the data scarcity and hydrogeological uncertainties. In this regard, Alps and Apennines have a different geological history that may affect the groundwater dynamics and this aspect may have not been glimpsed totally by the Dupuit model implemented in CRHyME. Unfortunately, the unavailability of reference piezometric data has not permitted us to assess model performance for this part.(Morbidelli et al., 2018)(Mishra et al., 2003)(ISPRA, 2018)Comparing volume and discharge scores a general tendency to overestimation of the peak discharge during rainfall seasons can be noticed while an underestimation of the discharges during winter is detected. The main reason should be imputed also in part to the water recirculation inside the groundwater reservoir that, as already anticipated in section 2, has been included bearing in mind several assumptions due to the data scarcity and hydrogeological uncertainties. In this regard, Alps and Apennines have a different geological history that may affect the groundwater dynamics and this aspect may have

not been glimpsed totally by the Dupuit model implemented in CRHyME. Unfortunately, the unavailability of reference piezometric data has not permitted us to assess model performance for this part.

4.1.1 Precipitation uncertainties: datasets across the Alps

Correctly assessing the precipitation distribution is mandatory to define a realistic representation of the external forcing that influences mainly the dynamic of the geo-hydrological cycle (Abbate et al., 2021b). Unfortunately, especially across mountain regions, the higher local variability of meteorology and the absence of a distributed network of stations can complicate the reconstruction of a continuous field, especially for rainfall. Differences were appreciated using two different datasets for the Valtellina case study, revealing that ARPA stations are settled ground-based and represent the most accurate indication of the effective rainfall drop into the soil surface. The former is the data required by CRHyME and in this sense, reanalysis data such as ones from MERIDA (Bonanno et al., 2019) are preferable because they already produce precipitation as a spatially distributed map, covering also area without rain gauges. Using MERIDA, we would expect a better performance from CRHyME runs but this hypothesis has not been confirmed in all situations. Looking at water volumes transited across the Fuentes hydrometer during the period 2015-2019, the MERIDA dataset has performed better than ARPA stations with respect to the reference. On the other hand, looking at the Mallero hydrometer, the MERIDA dataset has scored worse rather than using directly ARPA stations. What is the possible explanation for this contradictory fact?

The main difference resides in the different reconstructions of the rainfall field from the two datasets since the model has driven the simulations by keeping the same calibration parameters. MERIDA gives an already corrected rainfall map that has a spatial resolution of 4 km while the ARPA stations data are interpolated geometrically using the Inverse Distance Weight (IDW) techniques. The former is a good interpolator when the network density is rather high and uniformly distributed across the landscape and this is a good and fast solution for flat areas while across complex terrain, the orography can increase the errors in IDW (Abbate et al., 2021b). In the Valtellina case study, since it is a valley without a uniform rain gauge network, the IDW method has performed worse than MERIDA. Nevertheless, the power of MERIDA is valid if the watershed is rather large, while the performance may decrease for a smaller basin. In the Valtellina case study, this situation has emerged for the Mallero catchment (Figure 5) that represents a branch of the main reach Adda. Analysing the water discharge volume, across the Mallero basin, MERIDA has performed worse rather than IDW. In this case, the coarse resolution of MERIDA has represented a critical point while the rainfall field has been reconstructed in a better way by local ARPA stations. It is important to mention that the Mallero catchment is a well-monitored basin where around ~10 weather stations are distributed across an area of 320 km^2 so that IDW can interpolate better the precipitation field. This evidence is following some literature studies (Abbate et al., 2021b; Bonanno et al., 2019; Ly et al., 2013) where the problems related to the smoothing of the rainfall peak operating by meteorological models are highlighted.

4.1.2 Initial hydrological condition uncertainties

The choice of a realistic initial condition for the catchment's soil moisture and its dependence on rainfall field reconstruction represents a common problem for a deterministic model (Uber et al., 2018; Tramblay et al., 2010; Chow et al., 1988). In some cases, it is very difficult to have sufficient measures about the superficial water content of the soil, groundwater piezometric and superficial discharges. Regarding water flows, precise quantification of the discharge is generally produced by hydrometers that are normally located at the outlets of the basins. These data series are barely distributed and sometimes may fail to give useful data, especially during extreme events where they may be discontinued due to a lack of electric power. Finally, soil moisture is a quantity that can vary abruptly across different

terrain types, so it is not common to implement a network that permits the acquisition of distributed information across a catchment (Lazzari et al., 2018).

In CRHyME, these problems have been in part skipped considering that the model reached an automatic adjustment after some time steps that, depending on the extension of the basin, can be comprised of a few months up to some years. The former is a sort of automatic autocalibration of the model. In fact, the long-run simulation permits a distribution of the water across the cells of the domain (horizontally) and across each layer of the model (vertically). This effect was rather evident for the Emilia case study, where a realistic regime condition was reached only after a couple of years, and it was rather slower than for the Adda basin. The regime conditions have been acquired less rapidly since to the different soil compositions and morphology between the two areas. In the Apennines, the presence of clay can generally decrease the speed of soil saturation slowing down the groundwater recharge (Ronchetti et al., 2009; Ciccarese et al., 2020). As a result, the regime condition can take several times with respect to the Alps, where coarser terrain granulometry can reduce it due to higher soil permeabilities. Two-three years are generally sufficient to reach a regime condition since the fact that liquid discharge recorder at the outlets starts to match the hydrometric series.

4.2 The geo-hydrological performance of Valtellina and Emilia case studies

4.2.1 Solid Transport

Regarding the geo-hydrological hazard quantification, bearing in mind the limited availability of historical and reference data and their embedded uncertainties, landslide and solid transport processes have been reproduced with good affordability. The sediment yields calculated on a yearly based have been matched with respect to the available data of Tartano, Valgrosina and Cancano dams after a calibration procedure that has involved the application of the function for redistributing D_{50} grain size parameter across the catchment. The good reproduction of the annual sediment yield (~ 10% underestimation for Valtellina) has been confirmed also for the Emilia case study where the order of magnitude was correctly reproduced with respect to AdBPo reference (± 20% depending on the basin).

Since the D_{50} is embedded into the threshold that activates the sediment transport (Vetsch et al., 2018), it has revealed the critical parameter to be assessed in the CRHyME model. (ISPRA, 2018)(Inventario Fenomeni Franosi)(D'Agostino and Marchi, 2001)(Pérez Peña et al., 2009; Strahler, 1952)In the literature, there is plenty of studies that have investigated the dynamic of solid transport, but they lack giving a comprehensive theory that could be applied in those case where field data are not available. The empirical formulation proposed for CRHyME is an attempt in this direction, but since it is a currently open problem further research is planned for future versions of the model.

4.2.2 Shallow landslide and debris flow

The CRHyME model has identified correctly the localization and the timing of landslide failure during the extreme events that have affected the studied catchment. For the Valtellina area, 1987, 2000 and 2002 events were reproduced consistently by looking at ROC scores. The best scores were acquired for 2000 and 2002 events also a good quality census was available for the investigated area. For 1987, as can be appreciated in Figure 9, the incompleteness of the available census (yellow points) has affected the model's final score. However, independently from the specific case, the ROC methodology has permitted us

to highlight how the choice of stability parameters (friction angle and cohesion) has a critical influence on the final results. This fact has been confirmed also by the sensitivity analysis carried out for debris flow episodes in the Emilia case study during the event of 2014 and 2015. Here, in order to reach the best ROC scores with respect to the random classifier, the friction angles calibrated for Valtellina have been slightly reduced by about 20%.

CRHyME experience has shown how landslides and debris flow stability assessment cannot be treated deterministically even with an infinite slope model equation if some key data are not available or tuned indirectly from the others. In particular, the friction angle of the natural slope, and the cohesion of the superficial soil represent the most uncertain parameters that unfortunately cannot be estimated even if a terrain sample is analysed in the laboratory. The former cannot be properly done if the aim of the study is to investigate the slope stability at the catchment scale. Up to now, there are still few examples of the spatial distribution prediction of these two quantities that are essential for simulating geo-hydrological hazards, especially for landslide susceptibility mapping. In this regard, stochastic techniques are sometimes implemented to fulfil these needs (Vardon et al., 2016). In the simulations of Valtellina and Emilia case studies, a brief sensitivity analysis was carried out considering ranges given by the literature survey but without implementing a Montecarlo simulation of stability coefficients. The tuning procedure is difficult since (Hengl et al., 2017; Yu et al., 2018; Dade and Friend, 1998b; Chow et al., 1988)depends also on the large uncertainties that can be found inside the reference database that is used for validating the carried-out simulation. Moreover, friction angle depends on soil consolidation which is barely unknown while soil granulometry is the final result of the complex sediment dynamics and geological processes that have not been clarified at all (de Vente and Poesen, 2005; Merritt et al., 2003; Shobe et al., 2017; Ballio et al., 2010; Kondolf, 1997). Similarly, to the D_{50} parameter, these problems represent a research frontier that will be further strengthened in the future version of the model.

4.3 Geo-hydrological uncertainties: superficial geo-hydrological cycle

CRHyME is intended to simulate superficial geo-hydrological processes occurring at the catchment scale. Through a multi-hazard approach is possible to quantify these phenomena giving insight into their potential effects on the territory, useful for engineering and Civil Protection purpose. In this regard, CRHyME is one of the first examples of an integrated model.

The existing methodologies used in the engineering field have the main drawbacks of threatening separately geo-hydrological processes, not giving a comprehensive framework of the geo-hydrological cycle (ISPRA, 2018; Vetsch et al., 2018; Ali et al., 2019; Gariano and Guzzetti, 2016). In literature, models that assess jointly the erosion processes with shallow landslide instabilities at the catchment scale are rare (Baartman et al., 2012; Roo et al., 1996; Van Der Knijff et al., 2010) since the approaches adopted, the data required for simulations and their availability have historically limited the applicability inside a spatially-distributed model (Sutanudjaja et al., 2018; Strauch et al., 2018). Moreover, these processes have been studied in the past not always taking into account the high dynamicity of hydrological assessment, making strong assumptions on its stationarity, i.e. complete saturation of the slopes (Montgomery and Dietrich, 1994; Mandal and Maiti, 2015; Zhu and Xiao, 2020). In CRHyME, the hydrological aspect represents the main engine that, coherently with the observed reality, can trigger geo-hydrological instability at different locations and times.

Codice campo modificato

42

Thanks to the PCRaster functions, CRHyME is a tool that overcomes the limitation related to lumped parameter erosion model, stream power solid transport methodologies and to static susceptibility mapping for shallow landslide and debris flow. PCRaster permits to work with spatially distributed data and combine them to better describe the characteristic of a territory especially related to the local morphology, soil composition and coverages. Embedded routing functions are able to route the material (water or solid) through the whole catchment, extending the investigation of geo-hydrological in a spatial and time perspective. Processes are not evaluated at a specific river section or single slope under the hypothesis of stationarity, but they are simulating through the entire domain and considering their transient. Moreover, CRHyME could produce dynamic susceptibility maps, highlighting for shallow landslide phenomena the area that could destabilise at a particular time step of simulation, extending the concept of static susceptibility mapping where time components driven by meteorological triggering factors (rainfalls) are not always taken into account (Meisina et al., 2013; Ali et al., 2019; Atkinson and Massari, 1998; Benni Thiebes et al., 2017).

According to (Gariano and Guzzetti, 2016), reconstructing the whole geological cycle that drives the superficial erosion process and landslide formation is a challenge. CRHyME model is not an exception: EPM semi-quantitative model is considered for simulating the erosion process while landslide and debris flow triggering do not involve their runout. The runout processes can redistribute the local terrain changing the soil depth (asportation at the crown and accumulation at the toe) and modifying the DEM height. This dynamic is rather difficult to simulate consistently on a 2D domain even though a specific problem is addressed (Scheidl and Rickenmann, 2011). It represents one of the main assumptions for guaranteeing a fast functioning of the implemented routines in CRHyME: geo-hydrological assessment is computed after the hydrological assessment (one-directional sequence) and possible feedbacks, such as DEM modifications, are not taken into account up to now.

Uncertainties about hydrological simulations are present in CRHyME but can be "controlled" through the hydrometer stations if available locally. On the other hand, the assessment of the "superficial geological cycle" cannot be evaluated precisely since the monitoring of these geo-hydrological phenomena is still insufficient on a catchment scale (Inventario Fenomeni Franosi; ISPRA, 2018). Even though surface mapping and census are supposed to increase their accuracy and completeness in the future, some doubts remain about possible improvements in other fundamental data. To correctly assess the landslide triggering, a uniform soil layer cannot be sufficient sometimes but further information about local geology in terms of lithological material, strata inclination and immersion and the eventual presence of faults should be included to have a complete picture of dynamics and triggering of the local geo-hydrological processes (Montgomery and Dietrich, 1994; Bovolo and Bathurst, 2012; Cevasco et al., 2014; D'Amato Avanzi et al., 2004). Up to now, these data are still represented in the geological sections that depict an accurate profile of the possible configuration of the layers. Unfortunately, geological sections are not available digitally and cannot be included directly inside the models even though a complex 3D mesh is available and required by the program. The former is beyond the scope of CRHyME that can be in principle classified as a 2.5D model. Nevertheless, the possibility to include those data could help in interpreting superficial and groundwater fluxes to reduce uncertainties, especially for larger catchments. In this sense, the databases already adopted in CRHyME (Hengl et al., 2017; Huscroft et al.,

2018; Ross et al., 2018) have made an important homogenization of superficial soils properties that permit to implement in CRHyME stability models.

In conclusion, the deterministic reproduction of the "superficial geological cycle" poses some open problems still unresolved. Geo-hydrological processes cannot be perfectly coupled with the hydrological cycle since feedbacks are difficult to be taken into account and empirical formulations are necessary to try to simplify these complex interactions. CRHyME is one of the first attempts that aim to describe geo-hydrological processes coupled with hydrological dynamics deterministically and in an efficient way using the potentiality of PCRaster functions.

(Daly et al., 1997; Chow et al., 1988)(Abbate et al., 2021b)(Campforts et al., 2020; Bovy et al., 2020; Salles, 2019)(Sklar et al., 2017)5 Model Limitations

5 Conclusion

In engineering fields, geo-hydrogeological processes have been conventionally studied separately to make them more tractable for the sake of simplicity. Therefore, hydrological models that assess jointly the erosion, and sediment transport processes and evaluate shallow landslide instabilities are quite rare. In this sense, the CRHyME model was designed as a tool able to show a complete picture of the most significant geo-hydrological hazardsprocesses that may occur at the catchment scale.

In this work, the new model CRHyME and its applications are reported. CRHyME model was built ex-novo usingwith Python programming language, have the same framework and implementing faster PCRaster libraries that can simulate hydrological processes in a very efficient way. CRHyME includes some of the common features of the classical spatially distributed hydrological model but with an additionalits focusfocus is on quantitative reconstruction of geo-hydrological hazards. CRHyME is characterized by 6 modules that reproduce water hydrological balance over terrain and by a brand-new module deputed to simulate all the processes related to the geo-hydrological hazards (e.g. erosion, solid transport, shallow landslide and debris flow triggering at the catchment scale). In the field of geo-hydrological risk assessment, tCRHyME includes some of the common features of the classical hydrological model but with an additional focus on geo-hydrological hazards. Particular attention has been devoted to the study and to the implementation of the erosion and solid transport processes that can typically occur in a river catchment. Moreover, shallow landslide and debris flow stability models have been included. The integration of all those processes in a spatially distributed hydrological model represents a novelty in the field of geo-hydrological risk assessment. Of course, some hypotheses were assumed since it is quite impossible to implement accurately all the existent geo-hydrological mechanisms: some dynamics are still unknown or are too complex to be reduced to a 2D interpretation.

Since the aim of our study was to build and facilitate the usage of the model indistinctly in any area of the globe, a deep investigation of the open-source repositories available for initial data has been carried out. The user-defined calibration parameters have been reduced to the minimum. Among them, erosion coefficients, average sediment diameters, cohesion and

1205 friction angle have been tuned following the strategies presented above. A sensitivity analysis has been carried out to simplify and accelerate the reconstruction of realistic hydrological initial conditions, adding the possibility to activate the restart option after a spin-up period. Moreover, the DTM's resolution scale dependency was investigated and detected by the results. CRHyME was intensively tested to make it as general as possible and reproducible in whatever catchments.

~~A model is affordable if correctly calibrated and validated. Calibration procedures are a critical part of the most common~~
1210 ~~hydrological model since they measure how the results may be affected by the chosen parameters. Since the aim of our study was to build and use a model indistinctly in any area of the globe, the user-defined calibration parameters have been reduced to the minimum. In this way, we have reduced the possibility of parameter overfitting to a particular case study, making the CRHyME model rather general and usable in all catchments.~~ Our case studies, the of Caldone basin, the Valtellina Valley and the Emilia area, were chosen ~~with respect to~~looking at the availability of historical data that is of paramount importance for
1215 model validation. The results have shown a fairly good reproduction of the past observations: the model is hydrologically conservative (the volume of water recirculating across the basin is conserved), and numerically stable (thanks to PCRaster libraries); the solid discharge reproduced with downscaled EPM Gavrilovic's method is consistent with the observations, even though there are some uncertainties on D_{50} parameter; the triggering of shallow landslides and debris flows is comparable in number and spatial localization ~~with respect~~ to the census. However, CRHyME's performances are rather sensitive to the
1220 quality of rainfall field data that should be accurate in spatial and temporal resolution to allow the code to detect correctly possible triggered landslides.

The efforts conducted ~~in this study~~ with the creation of CRHyME go ~~are~~ in the direction of a better investigation ~~and reproduction~~ of geo-hydrological hazards. CRHyME is a multi-hazard model able to address and quantify at catchment scale several geo-hydrological processes that: may occur simultaneously, are physically ~~coupled and~~coupled and cannot be
1225 interpreted separately. With CRHyME is possible to overcome the software fragmentation that is currently present in the geo-hydrological field, answering the recent needs required for multi-hazard quantification and multi-risk evaluation not only for back analysis studies but also for now-casting evaluation at the Civil Protection level.

Appendix A

1230 Here, an example of the CRHyME ".INI" file ~~that was written for the computations~~for the simulation setting is reported. Each module has its own options where the parameters, variables and other settings required ~~for the model run~~ are specified. In the ".INI" file is essentially reported the simulation time settings (e.g., starting date and ending date), the spatially distributed input data and the meteorological and climatological data series, the settings of each computational module and the name of the output files. The ".INI" file is read by the "deterministic_runner.py" file that starts the CRHyME model and its internal
1235 routines: in "pre-processing.py", "reporting.py" and "plot.py" modules, variables are respectively defined, saved, and plotted following the formats and standards of the PCRaster libraries (Sutanudjaja et al., 2018; Karssenberg et al., 2010). CRHyME's results are reported in two formats, as a ".csv" datasheet or a ".netcdf" map (Jacob et al., 2014; Sutanudjaja et al., 2018). The first type is generally used to pick up information of a particular quantity at one location such as in the correspondence of a

rain gauge or hydrometric station. The datasheet is organized with a first column containing the time step value while the subsequent columns contain picked information of one or more monitoring points. The ".netcdf" maps are produced to store information about the states and fluxes variables of the model. At each timestep, the quantity at the spatial resolution of the DTM model is saved within the ".netcdf" stack. The required variable to be sampled should be specified in the ".INI" file under the "reporting options": for ".csv" files a ".map" file containing the location of samples points while for .netcdf the name of the variable required should be specified.

Using the GDAL libraries for Python (GDAL/OGR contributors, 2020), the input/output geographical data has been converted to the PCRaster standard format ".map" for raster data (Karssenberg et al., 2010; Sutanudjaja et al., 2018), considering WGS84 datum as a reference system for geographical projection. In the output's files: the lateral water fluxes $F_{sub}(t)$, $F_{GW}(t)$ and $F_{kin-dyn}(t)$ are converted into $[m^3 s^{-1}]$ considering the vertical section as a product of the cell width and respective storage height; the vertical water fluxes $C_I(t)$, $-S_{ml}(t)$, $I(t)$, $ETc(t)$, $R(t)$, $L_{per}(t)$, $Ex(t)$ and $Ex_{GW}(t)$ are expressed in $[mm\ day^{-1}]$; storage quantities $\Delta h_{snow}(t)$, $\Delta h_{soilwater}(t)$, $\Delta h_{groundwater}(t)$ and $\Delta h_{runoff}(t)$ are converted into $[m^3]$ for volumes simply multiplying the storage height by the cell area extension of the DTM in $[m^2]$. Further description of the sub-modules could be found inside the CRHyME's manual (Abbate and Mancusi, 2021a, b).

.INI FILE EXAMPLE

```
[globalOptions]                                              (CRHYME'S GENERAL OPTIONS)
inputDir = ***\ModelCRHyME\CRHyME_Inputs_Trebbia            (input directory)
outputDir = ***\ModelCRHyME\CRHyME_Outputs_R                (output directory)
cloneMap = map\clone.map                                    (clone map for delimiting domain)
landmask = None
institution = RSE_Ricerca Sistema Energetico                (institution name)
title = CRHyME project                                      (project title)
description = by Andrea Abbate and Leonardo Mancusi, resolution = 90 m   (project description)
resolution = 90                                             (spatial data resolution)
startSeries = 1985-12-31                                    (starting data of series)[1]
startTime = 1986-01-01                                      (starting data of simulation)[1]
endTime = 2005-12-30                                        (ending data of simulation)[1]
timestep = 24                                               (timestep resolution in hours)
startingStamp = 0
stampTimestep = 1                                           (stamp timestep in n° timestep)
Restart = 1                                                 (activate restart option after spin-up)
Restart_Snow = \restarts\mod2\Restart_Snow.map             (snow height state for restart)
Restart_Surface = \restarts\mod2\Restart_Surface.map       (runoff height state for restart)
Restart_Soil = \restarts\mod2\Restart_Soil.map             (soil water height state for restart)
Restart_Ground = \restarts\mod2\Restart_Ground.map         (ground water height state for restart)
```

46

```
       Restart_SoilSed = \restarts\mod2\Restart_SoilSed.map                (sediment height state for restart)

       [climaOptions]                                                       (CLIMA MODULE OPTIONS)
       CLIMA_Switch = 1                                                     (enable reanalysis-climatic input data)
1280   Rain_NC4 = netcdf\eucordhi_mod2_pr_day.nc                            (.netcf reanalysis-climatic input data)
       CorrectionFactor = 86400

       [meteoOptions]                                                       (METEO MODULE OPTIONS)
       input_tab = tab                                                      (folder containing .tab (txt) datasheet)
1285   mask = map\mask01.map                                                (0-1 mask map, equal to clone.map)
       DTM = map\DTM_clip.map                                               (elevation model dtm.map [m])
       z0 = tss\mod2\Z0_eucordhi_mod2_tas_day.tss                           (regression temp-elev: intercept)
       TempRatio = tss\mod2\TCoef_eucordhi_mod2_tas_day.tss                 (regression temp-elev: angular coeff.)
       z0MAX = tss\mod2\Z0_eucordhi_mod2_tasmax_day.tss                     (intercept for MAX temp.)
1290   TempRatioMAX = tss\mod2\TCoef_eucordhi_mod2_tasmax_day.tss           (angular coeff. for MAX temp.)
       z0MIN = tss\mod2\Z0_eucordhi_mod2_tasmin_day.tss                     (intercept for MIN temp.)
       TempRatioMIN = tss\mod2\TCoef_eucordhi_mod2_tasmin_day.tss           (angular coeff for MIN temp.)
       infilRain_file = tss\2011_2016\Rain_TREBBIA_Precipitazione_ALL.tss   (rain gauges time series .tss (txt))[2]
       mayrainstat = map\Rain_Stations_Trebbia.map                         (rain gauges location .map)[2]
1295   LAT = 43                                                             (latitude)
       ETC_Switch = 1                                                       (evapotranspiration calc. enabled)
       Aspect = map\Aspect_Filled.map                                       (aspect file .map [-])
       Slope = map\Slope_Filled.map                                         (slope file .map [-])
       mysoilmap = map\CLC_9Cat.map                                         (use of soil.map)
1300   Kc_FAO = tbl\Kc_FAO.tbl                                              (kc coefficient for FAO evapotras.)[3]
       Albedo = tbl\Albedo.tbl                                              (albedo coefficient for FAO evapotras.)[3]

       [interceptionSnowOptions]                                            (SNOW AND INTERCEPTION MODULE OPTIONS)
       input_tab = tab                                                      (folder containing .tab (txt) datasheet)
1305   LAImax = tbl\LAImax.tbl                                              (LAI maximum index)[4]
       LAImin = tbl\LAImin.tbl                                              (LAI minimum index)[4]
       SNOW_Switch = 1                                                      (snow calc. enabled)

       [landSurfaceOptions]                                                 (LAND SURFACE MODULE OPTIONS)
1310   input_tab = tab                                                      (folder containing .tab (txt) datasheet)
       INF_Switch = 2                                                       (infiltration calc. enabled)[5]
       sand_sup = map\Sand_SUP90C.map                                       (%sand on surface soil at 10cm depth)
       silt_sup = map\Silt_SUP90C.map                                       (%silt on surface soil at 10cm depth)
       clay_sup = map\Clay_SUP90C.map                                       (%clay on surface soil at 10cm depth)
1315   CoarseFrc_SUP = map\CoarsFrg_SUP90C.map                              (%coarse on surface soil at 10cm depth)
       myrivermap = map\PathRiverSM.map                                     (river location .map)[6]
```

```
        Loss_River = tbl\Loss_RIV.tbl                          (reduction coeff. for river losses)6
        Inf_CLC = tbl\Infiltr_CLC.tbl                          (infiltration coeff. f(soil use))
        CN_I = map\CN_I.map                                    (SCS-CN method CN I .map)
1320    CN_II = map\CN_II.map                                  (SCS-CN method CN II .map)
        CN_III = map\CN_III.map                                (SCS-CN method CN III .map)
        Initial_SM = 0.9                                       (initial condition of soil moisture)
        SoilDepth = map\BDRICM_M.map                           (soil depth .map [cm])
        MaxWatStgTOP = map\TSH1_clip.map                       (%max water storage soil 10cm depth)
1325
        MaxWatStgBTM = map\TSH5_clip.map                       (%max water storage soil 1m depth)
        sand_btm = map\Sand_BTM90C.map                         (%sand on surface soil at 1m depth)
        silt_btm = map\Silt_BTM90C.map                         (%silt on surface soil at 1m depth)
        clay_btm = map\Clay_BTM90C.map                         (%clay on surface soil at 1m depth)
1330    CoarseFrc_BTM = map\CoarsFrg_BTM90C.map                (%coarse on surface soil at 1m depth)


        [groundwaterOptions]                                   (GROUNDWATER MODULE OPTIONS)
        input_tab = tab                                        (folder containing .tab (txt) datasheet)
        Sr_Falda = 0.8                                         (initial condition of groundwater table)
1335    Idro_Map = map\Idrogeology_Emilia_Trebbia.map          (hydrogeological .map)7
        Ks_GLHYMPS_exp = map\GLHYMPS_Emilia_Trebbia.map        (saturated permeability from GLHYMPS)7
        Permeability = tbl\IdrogeologyTabs\Permeability.tbl    (saturated permeability .tbl (txt))7
        Anisotrophy = tbl\IdrogeologyTabs\Anisotrophy.tbl      (anisotropy coefficient .tbl (txt))7
        Porosity = tbl\IdrogeologyTabs\Porosity.tbl            (porosity coefficient .tbl (txt))7
1340    Storativity = tbl\IdrogeologyTabs\Storativity.tbl      (storativity coefficient .tbl (txt))7
        Type_Depth = tbl\IdrogeologyTabs\Type.tbl              (hydrogeological reclassify .tbl(txt))7


        [LandSlidesOptions]                                    (LANDSLIDE MODULE OPTIONS)
        LANDSLIDE_Switch_1 = 2                                 (landslide trigger calc. enabled)8
1345    C_Veg = tbl\C_Veg.tbl                                  (cohesion from vegetation .tbl(txt))
        Surcharge = tbl\Sur_Veg.tbl                            (cohesion from vegetation .tbl(txt))
        fa_factor = 2
        X_Gavrilovic = tbl\X_Gavrilovic.tbl                    (EPM X parameter .tbl(txt))9
        Y_Gavrilovic = tbl\Y_Gavrilovic.tbl                    (EPM Y parameter .tbl(txt))9
1350    LithoY_Gavrilovic = map\Idrogeology_Emilia_Trebbia.map (EPM Y parameter lithology .map)9
        FI_Gavrilovic = map\Kst_Emilia_Trebbia.map            (EPM fi parameter .map)9


        [routingOptions]                                       (ROUTING MODULE OPTIONS)
        ROUTING_Switch = 1                                     (enable calc. routing)
1355    lddMap = map\ldd_clip.map                              (ldd.map of flow directions)
        cellAreaMap = map\cellsizeArea.map                     (map of cell area extension)
        River_Pit = map\Pit_Point.map                         (basin outlet location)
```

48

```
        Strickler = tbl\Ks_Strickler.tbl                        (Strickler-Manning coefficient)
        SectionTable = tbl\Dynamic\Sections2.tbl                (section type table .map)[10]
1360    RiverDynPath = tbl\Dynamic\map\PathDyn.map
        RiverDynDist = tbl\Dynamic\map\DistDyn.map
        RiverDynPit = tbl\Dynamic\map\Pit_Point.map
        RiverDynPitLake = tbl\Dynamic\map\Pit_Point_Lakes_IN.map


1365    [reportingOptions]                                      (REPORTING MODULE OPTIONS)
        mysamples_real = map\Idro_Samples_Trebbia.map           (real hydrometers sampling .map)
        mysamples_fake = map\Idro_Samples_F.map                 (other hydrometers sampling .map)
        mysamples_solid = map\Solid_Samples.map                 (reservoir sampling .map)
        debugmode = FAST
1370    outDailyTotNC = CumFails,CumFails_D,P                    (daily counted .netcdf)
        outMonthTotNC = P,Etc                                   (monthly counted .netcdf)
        outMonthAvgNC = T                                       (monthly averaged .netcdf)
        outMonthEndNC = CumFails,CumFails_D                     (end-monthly counting .netcdf)
        outAnnualTotNC = P,Etc                                  (annual cumulated .netcdf)
1375    outAnnualAvgNC = T                                      (monthly averaged .netcdf)
        outAnnuaEndNC = CumFails,CumFails_D                     (end-annual cumulated .netcdf)
        #debugmode = SLOW
        #outDailyTotNC = P,T,ETc,DeltaWS0,Sr3,DeltaBF0,FS,CumFails,FS_D,CumFails_D,FS_ST,CumFails_ST
        formatNetCDF = NETCDF4                                  (.netcdf specified format)
1380    zlib = True                                             (enable .netcdf creation)
```

ID	Description	Module	Additional References
1	Are specified the starting point of the time series, the starting point of the simulation and the ending point.	[GLOBAL OPTIONS]	-
2	To compute rain gauge simulation, time series in .tss format and a .map of stations are required. Each station has its IDs (1,2,3,…,n) for the corresponding time series with map.	[METEO OPTIONS]	(Karssenberg et al., 2010; Sutanudjaja et al., 2018)
3-4	Fao crop coefficient Kc, albedo coefficient and LAI coefficient within .tbl file (a txt table).	[METEO OPTIONS] – [INTERCEPTION SNOW OPTIONS]	(Allan et al., 1998; Nazari et al., 2019)
5	Infiltration model selector: 1) Horton, 2) SCS-SN	[LANDURFACE OPTIONS]	(Chow et al., 1988)
6	River map derived from PCR flow accumulation and percolation reduction factor below riverbed path.	[LANDURFACE OPTIONS]	(Chow et al., 1988)
7	Groundwater parameters (.tbl), lithology map and saturated permeability map retrieved from literature and GHYMPS database.	[GROUNDWATER OPTIONS]	(Huscroft et al., 2018; Anderson, 2005; Hayashi, 2020; de Graaf et al., 2015b)

49

8	Landslide model selector: 1) Iverson, 2) Harp, 3) Milledge and 4) SLIP	[LANDSLIDE OPTIONS]	(Iverson, 2000; Montrasio, 2008; Harp et al., 2006; Milledge et al., 2014)
9	EPM parameters from Gavrilovic's method (.tbl and .map)	[LANDSLIDE OPTIONS]	(Milanesi et al., 2015; Panagos et al., 2015)
10	Section table (.tbl) requires for implementation of dynamic routing (experimental)	[ROUTING OPTIONS]	(Karssenberg et al., 2010; Sutanudjaja et al., 2018)

Appendix B

385 Here are reported all the symbols and their units of measure included in the CRHyME model (Abbate and Mancusi, 2021a, b).

Main symbols	Description	Units of measurement
A	Hydraulic section area	m^2
B	Width of the hydraulic section	m
c	Cohesion of surface soils	kPa
C^*	Concentration of debris flows	-
C_i	Canopy Interception	mm day^{-1}
CNI CNII CNIII	Curve Numbers SCS-CN for dry-mild-wet conditions	-
D_{50}	Median diameter of soil grain size	mm
ddf_0	Degree day factor	mm °C^{-1} day^{-1}
E_s	Surface erosion	mm timestep^{-1}
Et_0	Potential evapotranspiration	mm
Et_c	Evapotranspiration	mm timestep^{-1}
E_x	Exfiltration	mm timestep^{-1}
f_0	Maximum infiltration rate of Horton	mm h^{-1}
f_c	Horton's minimum infiltration rate	mm h^{-1}
F_{gw}	Groundwater flow	$m^3 s^{-1}$
F_{sub}	Subsurface flow	$m^3 \, s^{-1}$
$depth_{GW}$	Groundwater depth	mm
$depth_{Soil}$	Surface soil depth	mm
h_{snow}	Snow height	mm
h_{runoff}	Water height at surface	mm
$h_{soilwater}$	Water height in surface soil	mm
$h_{groundwater}$	Water height in aquifer	mm

h_{solid}	Solid height at surface	mm
i o S	Dimensionless slope and degrees	% or °
I_a	Initial imbibition of the SCS-CN method	mm
k	Horton decay constant	h^{-1}
K_c	Crop Coefficient	-
K_s	Hydraulic permeability	$m\ s^{-1}$
K_{str}	Strickler roughness coefficient	-
LAI	Leaf Area Index	-
L_{per}	Percolation	mm timestep^{-1}
n	Porosity	-
n_{VG}	Van Genucten n parameter	-
n_{str}	Manning coefficient	-
P	Rainfall	mm timestep^{-1}
P_n	Net Rainfall	mm timestep^{-1}
Q o ql	Liquid Discharge	$m^3\ s^{-1}$
qc	Critical flow rate of incipient motion for solids	$m^3\ s^{-1}$
qs	Solid flow rate	$m^3\ s^{-1}$
R	Runoff	$m^3\ s^{-1}$
S	Snow	mm
S_{tor}	SCS-CN Storativity	mm
S_{ml}	Snowmelt	mm timestep^{-1}
S_m	Soil Moisture	%
T	Temperature	°C
T_{max} e T_{min}	Maximum and minimum temperature	°C
T_s	Solid Transport	$m^3\ s^{-1}$
α e β liquido	Parameters of the uniform (liquid) flow rate curve	-
α e β solido	Parameters of the uniform (solid) flow rate curve	-
φ	Friction angle of surface soils	°
θ_s e θ_r	Maximum and minimum surface soil water content	mm or %

References

1390 Abbate, A. and Mancusi, L.: Manuale del modello CRHyME (Climate Rainfall Hydrogeological Modelling Experiment), RSE Report RdS 21012462, Milano, 2021a.

Abbate, A. and Mancusi, L.: Strumenti per la mappatura delle minacce idrogeologiche per il sistema energetico e incidenza dei cambiamenti climatici, RSE Report RdS 21010317, Milano, 2021b.

Abbate, A., Longoni, L., Ivanov, V. I., and Papini, M.: Wildfire impacts on slope stability triggering in mountain
1395 areas, MDPI Geosciences, 9, 1–15, https://doi.org/10.3390/geosciences9100417, 2019.

Abbate, A., Papini, M., and Longoni, L.: Analysis of meteorological parameters triggering rainfall-induced landslide: a review of 70 years in Valtellina, Nat. Hazards Earth Syst. Sci., 21, 2041–2058, https://doi.org/10.5194/nhess-21-2041-2021, 2021a.

Abbate, A., Longoni, L., and Papini, M.: Extreme Rainfall over Complex Terrain: An Application of the Linear
1400 Model of Orographic Precipitation to a Case Study in the Italian Pre-Alps, 2021, MDPI Geosciences, 18, 2021b.

Abeshu, G. W., Li, H.-Y., Zhu, Z., Tan, Z., and Leung, L. R.: Median bed-material sediment particle size across rivers in the contiguous U.S., Earth Syst. Sci. Data Discuss., 2021, 1–22, https://doi.org/10.5194/essd-2021-201, 2021.

Allan, R., Pereira, L., and Smith, M.: Crop evapotranspiration-Guidelines for computing crop water requirements-
1405 FAO Irrigation and drainage paper 56, 1998.

Alvioli, M., Melillo, M., Guzzetti, F., Rossi, M., Palazzi, E., von Hardenberg, J., Brunetti, M. T., and Peruccacci, S.: Implications of climate change on landslide hazard in Central Italy, Science of The Total Environment, 630, 1528–1543, https://doi.org/10.1016/j.scitotenv.2018.02.315, 2018.

Ancey, C.: Bedload transport: a walk between randomness and determinism. Part 1. The state of the art, null, 58,
1410 1–17, https://doi.org/10.1080/00221686.2019.1702594, 2020.

Anderson, E. I.: Modeling groundwater–surface water interactions using the Dupuit approximation, Advances in Water Resources, 28, 315–327, https://doi.org/10.1016/j.advwatres.2004.11.007, 2005.

Angeli, M. G., Buma, J., Gasparetto, P., and Pasuto, A.: A combined hill slope hydrology/stability model for low-gradient slopes in the Italian Dolomites, Engineering Geology, 49, 1–13, https://doi.org/10.1016/S0013-
1415 7952(97)00033-1, 1998.

Rete Monitoraggio ARPA Emilia: https://www.arpae.it/it/temi-ambientali/meteo.

Rete Monitoraggio ARPA Lombardia: www.arpalombardia.it/stiti/arpalombardia/meteo.

Autorità di Bacino Distrettuale del Fiume Po: Linee Generali di Assetto Idrogeologico e Quadro degli Interventi, 2022.

1420 Ballio, F., Brambilla, D., Giorgetti, E., Longoni, L., Papini, M., and Radice, A.: Evaluation of sediment yield from valley slopes: A case study, 149 pp., https://doi.org/10.2495/DEB100131, 2010.

Bancheri, M., Rigon, R., and Manfreda, S.: The GEOframe-NewAge Modelling System Applied in a Data Scarce Environment, Water, 12, https://doi.org/10.3390/w12010086, 2020.

Barnes, R.: Parallel Priority-Flood depression filling for trillion cell digital elevation models on desktops or clusters,
1425 Computers & Geosciences, 96, 56–68, https://doi.org/10.1016/j.cageo.2016.07.001, 2016.

Barnes, R.: Parallel non-divergent flow accumulation for trillion cell digital elevation models on desktops or clusters, Environmental Modelling & Software, 92, 202–212, https://doi.org/10.1016/j.envsoft.2017.02.022, 2017.

Bemporad, G. A., Alterach, J., Amighetti, F. F., Peviani, M., and Saccardo, I.: A distributed approach for sediment yield evaluation in Alpine regions, Journal of Hydrology, 197, 370–392, https://doi.org/10.1016/0022-
1430 1694(95)02978-8, 1997.

Berg, J. H.: Prediction of Alluvial Channel Pattern of Perennial Rivers, Geomorphology, 12, 259–279, https://doi.org/10.1016/0169-555X(95)00014-V, 1995.

Bonanno, R., Lacavalla, M., and Sperati, S.: A new high-resolution Meteorological Reanalysis Italian Dataset: MERIDA, Quarterly Journal of the Royal Meteorological Society, 145, 1756–1779,
1435 https://doi.org/10.1002/qj.3530, 2019.

Bordoni, M., Meisina, C., Valentino, R., Lu, N., Bittelli, M., and Chersich, S.: Hydrological factors affecting rainfall-induced shallow landslides: From the field monitoring to a simplified slope stability analysis, Engineering Geology, 193, https://doi.org/10.1016/j.enggeo.2015.04.006, 2015.

Bovolo, C. I. and Bathurst, J. C.: Modelling catchment-scale shallow landslide occurrence and sediment yield as a
1440 function of rainfall return period, Hydrological Processes, 26, 579–596, https://doi.org/10.1002/hyp.8158, 2012.

Bovy, B., Braun, J., Cordonnier, G., Lange, R., and Yuan, X.: The FastScape software stack: Reusable tools for landscape evolution modelling, in: EGU General Assembly Conference Abstracts, 9474, 2020.

Bozzolan, E., Holcombe, E., Pianosi, F., and Wagener, T.: Including informal housing in slope stability analysis – an application to a data-scarce location in the humid tropics, Natural Hazards and Earth System Sciences, 20, 3161–
1445 3177, https://doi.org/10.5194/nhess-20-3161-2020, 2020.

Brambilla, D., Papini, M., Ivanov, V. I., Bonaventura, L., Abbate, A., and Longoni, L.: Sediment Yield in Mountain Basins, Analysis, and Management: The SMART-SED Project, in: Applied Geology: Approaches to Future Resource Management, edited by: De Maio, M. and Tiwari, A. K., Springer International Publishing, Cham, 43–59, https://doi.org/10.1007/978-3-030-43953-8_3, 2020.

Bresciani, E., Davy, P., and de Dreuzy, J.-R.: Is the Dupuit assumption suitable for predicting the groundwater seepage area in hillslopes?, Water Resources Research, 50, 2394–2406, https://doi.org/10.1002/2013WR014284, 2014.

Campforts, B., Shobe, C., Steer, P., Vanmaercke, M., LAGUE, D., and Braun, J.: HyLands 1.0: a Hybrid Landscape evolution model to simulate the impact of landslides and landslide-derived sediment on landscape evolution, Geoscientific Model Development, 13, 3863–3886, 2020.

Cazorzi, F. and Dalla Fontana, G.: Snowmelt modelling by combining air temperature and a distributed radiation index, Journal of Hydrology, 181, 169–187, https://doi.org/10.1016/0022-1694(95)02913-3, 1996.

Ceriani, M., Lauzi, S., and Padovan, M.: Rainfall thresholds triggering debris-flow in the alpine area of Lombardia Region, central Alps – Italy, in: In Proceedings of the Man and Mountain'94, First International Congress for the Protection and Development of Mountain Environmen, Ponte di Legno (BS), Italy, 1994.

Chen, L. and Young, M. H.: Green-Ampt infiltration model for sloping surfaces, Water Resources Research, 42, https://doi.org/10.1029/2005WR004468, 2006.

Chow, V. T., Maidment, D. R., and Mays, L. W.: Applied hydrology, McGraw-Hill, New York, 1988.

Ciccarese, G., Mulas, M., Alberoni, P. P., Truffelli, G., and Corsini, A.: Debris flows rainfall thresholds in the Apennines of Emilia-Romagna (Italy) derived by the analysis of recent severe rainstorms events and regional meteorological data, Geomorphology, 358, 107097, https://doi.org/10.1016/j.geomorph.2020.107097, 2020.

Cislaghi, A., Chiaradia, E. A., and Bischetti, G. B.: Including root reinforcement variability in a probabilistic 3D stability model, Earth Surface Processes and Landforms, 42, 1789–1806, https://doi.org/10.1002/esp.4127, 2017.

CNR and IRPI: Rapporto Periodico sul Rischio posto alla Popolazione italiana da Frane e Inondazioni, Anno 2020, 19 pp., https://doi.org/10.30437/report2020, 2021.

Collischonn, W., Fleischmann, A., Paiva, R. C. D., and Mejia, A.: Hydraulic Causes for Basin Hydrograph Skewness, Water Resources Research, 53, 10603–10618, https://doi.org/10.1002/2017WR021543, 2017.

Crosta, G. B., Imposimato, S., and Roddeman, D. G.: Numerical modelling of large landslides stability and runout, Nat. Hazards Earth Syst. Sci., 3, 523–538, https://doi.org/10.5194/nhess-3-523-2003, 2003.

Dade, W. B. and Friend, P. F.: Grain-Size, Sediment-Transport Regime, and Channel Slope in Alluvial Rivers, The Journal of Geology, 106, 661–676, https://doi.org/10.1086/516052, 1998a.

Dade, W. B. and Friend, P. F.: Grain-Size, Sediment-Transport Regime, and Channel Slope in Alluvial Rivers, The Journal of Geology, 106, 661–676, https://doi.org/10.1086/516052, 1998b.

D'Agostino, V. and Marchi, L.: Debris flow magnitude in the Eastern Italian Alps: Data collection and analysis, Physics and Chemistry of the Earth, Part C: Solar, Terrestrial & Planetary Science, 26, 657–663, https://doi.org/10.1016/S1464-1917(01)00064-2, 2001.

Daly, C., Taylor, G., and Gibson, W.: The PRISM Approach to Mapping Precipitation and Temperature, 1997.

Daly, C., Slater, M. E., Roberti, J. A., Laseter, S. H., and Swift Jr, L. W.: High-resolution precipitation mapping in a mountainous watershed: ground truth for evaluating uncertainty in a national precipitation dataset, International Journal of Climatology, 37, 124–137, https://doi.org/10.1002/joc.4986, 2017.

De Vita, P., Fusco, F., Tufano, R., and Cusano, D.: Seasonal and Event-Based Hydrological and Slope Stability Modeling of Pyroclastic Fall Deposits Covering Slopes in Campania (Southern Italy), Water, 10, 1140, https://doi.org/10.3390/w10091140, 2018.

Devia, G. K., Ganasri, B. P., and Dwarakish, G. S.: A Review on Hydrological Models, Aquatic Procedia, 4, 1001–1007, https://doi.org/10.1016/j.aqpro.2015.02.126, 2015.

Erskine, R. H., Green, T. R., Ramirez, J. A., and MacDonald, L. H.: Comparison of grid-based algorithms for computing upslope contributing area, Water Resources Research, 42, https://doi.org/10.1029/2005WR004648, 2006.

Fan, Y., Miguez-Macho, G., Weaver, C. P., Walko, R., and Robock, A.: Incorporating water table dynamics in climate modeling: 1. Water table observations and equilibrium water table simulations, Journal of Geophysical Research: Atmospheres, 112, https://doi.org/10.1029/2006JD008111, 2007.

Fawcett, T.: An introduction to ROC analysis, Pattern Recognition Letters, 27, 861–874, https://doi.org/10.1016/j.patrec.2005.10.010, 2006.

Formetta, G., Capparelli, G., and Versace, P.: Evaluating performance of simplified physically based models for shallow landslide susceptibility, Hydrology and Earth System Sciences, 20, 4585–4603, https://doi.org/10.5194/hess-20-4585-2016, 2016.

G., C., M., M., and A., C.: Combining spatial modelling and regionalization of rainfall thresholds for debris flows hazard mapping in the Emilia-Romagna Apennines (Italy), Landslides, 18, 3513–3529, https://doi.org/10.1007/s10346-021-01739-w, 2021.

Gao, L., Zhang, L. M., and Cheung, R. W. M.: Relationships between natural terrain landslide magnitudes and triggering rainfall based on a large landslide inventory in Hong Kong, Landslides, 15, 727–740, https://doi.org/10.1007/s10346-017-0904-x, 2018.

Gariano, S. L. and Guzzetti, F.: Landslides in a changing climate, Earth-Science Reviews, 162, 227–252, https://doi.org/10.1016/j.earscirev.2016.08.011, 2016.

GDAL/OGR contributors: GDAL/OGR Geospatial Data Abstraction software Library, Open Source Geospatial Foundation, 2020.

Girard, M.-C., Girard, C., Dominique, C., Gilliot, J.-M., Loubersac, L., Meyer-Roux, J., Monget, J.-M., Seguin, B., and Rao, N.: Corine Land Cover, 331–344, https://doi.org/10.1201/9780203741917-19, 2018.

Gleick, P. H.: Climate change, hydrology, and water resources, Reviews of Geophysics, 27, 329–344, https://doi.org/10.1029/RG027i003p00329, 1989.

Globevnik, L., Holjevj_, D., Petkowaek, G., and Rubinj_, J.: 145. Applicability of the Gavrilo vic Method in Erosion Calculation Using Spatial Data Manipulation Techniques, Tunnelling and Underground Space Technology, 14, 2003.

Govers, G.: Empirical relationships for the transport capacity of overland flow., 1989.

Govers, G., Wallings, D. E., Yair, A., and Berkowicz, S.: Empirical relationships for the transport capacity of overland flow, International Association of Hydrological Sciences, 189, 1990.

de Graaf, I. E. M., Sutanudjaja, E. H., van Beek, L. P. H., and Bierkens, M. F. P.: A high-resolution global-scale groundwater model, Hydrol. Earth Syst. Sci., 19, 823–837, https://doi.org/10.5194/hess-19-823-2015, 2015a.

de Graaf, I. E. M., Sutanudjaja, E. H., van Beek, L. P. H., and Bierkens, M. F. P.: A high-resolution global-scale groundwater model, Hydrol. Earth Syst. Sci., 19, 823–837, https://doi.org/10.5194/hess-19-823-2015, 2015b.

Groenendyk, D. G., Ferré, T. P. A., Thorp, K. R., and Rice, A. K.: Hydrologic-Process-Based Soil Texture Classifications for Improved Visualization of Landscape Function., PLoS One, 10, e0131299, https://doi.org/10.1371/journal.pone.0131299, 2015.

Guadagno, M., IRPI CNR, P., Guzzetti, I., Reichenbach, I., and Tonelli, I.: SICI-Sistema Informativo Catastrofi Idrogeologiche-Istituto di Ricerca per la Protezione Idrogeologica (IRPI) del Consiglio Nazionale delle Ricerche e Gruppo Nazionale per la Difesa dalle Catastrofi Idrogeologiche (GNDCI) del Consiglio Nazionale delle Ricerche, 2003.

Gudiyangada Nachappa, T., Tavakkoli Piralilou, S., Ghorbanzadeh, O., Shahabi, H., and Blaschke, T.: Landslide Susceptibility Mapping for Austria Using Geons and Optimization with the Dempster-Shafer Theory, Applied Sciences, 9, https://doi.org/10.3390/app9245393, 2019.

Guzzetti, F. and Tonelli, G.: Information system on hydrological and geomorphological catastrophes in Italy (SICI): a tool for managing landslide and flood hazards, Natural Hazards and Earth System Sciences, 4, 213–232, 2004.

Guzzetti, F., Reichenbach, P., Cardinali, M., Galli, M., and Ardizzone, F.: Probabilistic landslide hazard assessment at the basin scale, Geomorphology, 72, 272–299, https://doi.org/10.1016/j.geomorph.2005.06.002, 2005.

Guzzetti, F., Peruccacci, S., Rossi, M., and Stark, C. P.: Rainfall thresholds for the initiation of landslides in central and southern Europe, Meteorology and Atmospheric Physics, 98, 239–267, https://doi.org/10.1007/s00703-007-0262-7, 2007.

Harp, E. L., Michael, J. A., and Laprade, W. T.: Shallow-landslide hazard map of Seattle, Washington, Reston, VA, https://doi.org/10.3133/ofr20061139, 2006.

Hayashi, M.: Alpine Hydrogeology: The Critical Role of Groundwater in Sourcing the Headwaters of the World, Groundwater, 58, 498–510, https://doi.org/10.1111/gwat.12965, 2020.

Hengl, T., Mendes de Jesus, J., Heuvelink, G. B. M., Ruiperez Gonzalez, M., Kilibarda, M., Blagotić, A., Shangguan, W., Wright, M. N., Geng, X., Bauer-Marschallinger, B., Guevara, M. A., Vargas, R., MacMillan, R. A., Batjes, N. H., Leenaars, J. G. B., Ribeiro, E., Wheeler, I., Mantel, S., and Kempen, B.: SoilGrids250m: Global gridded soil information based on machine learning, PLOS ONE, 12, e0169748, https://doi.org/10.1371/journal.pone.0169748, 2017.

Herrera, M.: Landslide Detection using Random Forest Classifier, https://doi.org/10.13140/RG.2.2.31365.91369, 2019.

Huscroft, J., Gleeson, T., Hartmann, J., and Börker, J.: Compiling and Mapping Global Permeability of the Unconsolidated and Consolidated Earth: GLobal HYdrogeology MaPS 2.0 (GLHYMPS 2.0), Geophysical Research Letters, 45, https://doi.org/10.1002/2017GL075860, 2018.

ISPRA: Dissesto idrogeologico in Italia: pericolosità e indicatori di rischio, ISPRA, Ispra, 2018.

ITCOLD: La gestione dell'interrimento dei serbatoi artificiali italiani, Comitato Nazionale Italiano delle Grandi Dighe, 2009.

ITCOLD: La gestione dell'interrimento dei serbatoi artificiali italiani situazione attuale e prospettive, Comitato Nazionale Italiano delle Grandi Dighe, 2016.

Ivanov, V., Radice, A., Papini, M., and Longoni, L.: Event-scale pebble mobility observed by RFID tracking in a pre-Alpine stream: a field laboratory, Earth Surface Processes and Landforms, 45, 535–547, https://doi.org/10.1002/esp.4752, 2020a.

Ivanov, V., Arosio, D., Tresoldi, G., Hojat, A., Zanzi, L., Papini, M., and Longoni, L.: Investigation on the Role of Water for the Stability of Shallow Landslides-Insights from Experimental Tests, Water, 12(4), 2020b.

Iverson, R., Reid, M., and Lahusen, R.: Debris-flow mobilization from landslides. Annu Rev Earth Planet Sci, Annu. Rev. Earth Planet. Sci, 25, 85–138, https://doi.org/10.1146/annurev.earth.25.1.85, 1997.

Iverson, R. M.: Landslide triggering by rain infiltration, Water Resources Research, 36, 1897–1910, https://doi.org/10.1029/2000WR900090, 2000.

Jackson, C. R., Bitew, M., and Du, E.: When interflow also percolates: downslope travel distances and hillslope process zones, Hydrological Processes, 28, 3195–3200, https://doi.org/10.1002/hyp.10158, 2014.

Jacob, D., Petersen, J., Eggert, B., Alias, A., Christensen, O. B., Bouwer, L. M., Braun, A., Colette, A., Déqué, M., Georgievski, G., Georgopoulou, E., Gobiet, A., Menut, L., Nikulin, G., Haensler, A., Hempelmann, N., Jones, C., Keuler, K., Kovats, S., Kröner, N., Kotlarski, S., Kriegsmann, A., Martin, E., van Meijgaard, E., Moseley, C., Pfeifer, S., Preuschmann, S., Radermacher, C., Radtke, K., Rechid, D., Rounsevell, M., Samuelsson, P., Somot, S., Soussana, J.-F., Teichmann, C., Valentini, R., Vautard, R., Weber, B., and Yiou, P.: EURO-CORDEX: new high-

resolution climate change projections for European impact research, Regional Environmental Change, 14, 563–578, https://doi.org/10.1007/s10113-013-0499-2, 2014.

Jakob, M. and Hungr, O.: Debris-Flow Hazards and Related Phenomena, 2005.

Jakob, M. and Jordan, P.: Design flood estimates in mountain streams – the need for a geomorphic approach, Can. J. Civ. Eng., 28, 425–439, https://doi.org/10.1139/l01-010, 2001.

Jie, T., Zhang, B., He, C., and Yang, L.: Variability In Soil Hydraulic Conductivity And Soil Hydrological Response Under Different Land Covers In The Mountainous Area Of The Heihe River Watershed, Northwest China, Land Degradation & Development, 28, https://doi.org/10.1002/ldr.2665, 2016.

Kadavi, P., Lee, C.-W., and Lee, S.: Application of Ensemble-Based Machine Learning Models to Landslide Susceptibility Mapping, Remote Sensing, 10, 1252, https://doi.org/10.3390/rs10081252, 2018.

Karssenberg, D., Schmitz, O., Salamon, P., de Jong, K., and Bierkens, M. F. P.: A software framework for construction of process-based stochastic spatio-temporal models and data assimilation, Environmental Modelling & Software, 25, 489–502, https://doi.org/10.1016/j.envsoft.2009.10.004, 2010.

Kim, K.-S., Kim, M.-I., Lee, M.-S., and Hwang, E.-S.: Regression Equations for Estimating Landslide-Triggering Factors Using Soil Characteristics, Applied Sciences, 10, https://doi.org/10.3390/app10103560, 2020.

Klaus, J. and Jackson, C. R.: Interflow Is Not Binary: A Continuous Shallow Perched Layer Does Not Imply Continuous Connectivity, Water Resources Research, 54, 5921–5932, https://doi.org/10.1029/2018WR022920, 2018.

Kobierska, F., Jonas, T., Kirchner, J. W., and Bernasconi, S. M.: Linking baseflow separation and groundwater storage dynamics in an alpine basin (Dammagletscher, Switzerland), Hydrol. Earth Syst. Sci., 19, 3681–3693, https://doi.org/10.5194/hess-19-3681-2015, 2015.

Kondolf, george 'mathias: Hungry Water: Effects of Dams and Gravel Mining on River Channels, Environmental Management, 21, 533–551, https://doi.org/10.1007/s002679900048, 1997.

Lamb, M. P. and Venditti, J. G.: The grain size gap and abrupt gravel-sand transitions in rivers due to suspension fallout, Geophysical Research Letters, 43, 3777–3785, https://doi.org/10.1002/2016GL068713, 2016.

Langland, M. J.: Bathymetry and Sediment-Storage Capacity Change in Three Reservoirs on the Lower Susquehanna River, 1996-2008, https://doi.org/10.3133/sir20095110, 2009.

Lazzari, M., Piccarreta, M., and Manfreda, S.: The role of antecedent soil moisture conditions on rainfall-triggered shallow landslides, Natural Hazards and Earth System Sciences Discussions, 2018, 1–11, https://doi.org/10.5194/nhess-2018-371, 2018.

Lee, K. and Pin Chun, H.: Evaluating the adequateness of kinematic-wave routing for flood forecasting in midstream channel reaches of Taiwan, Journal of Hydroinformatics, 14, 1075, https://doi.org/10.2166/hydro.2012.093, 2012.

Lehner, B., Verdin, K., and Jarvis, A.: New Global Hydrography Derived From Spaceborne Elevation Data, Eos, Transactions American Geophysical Union, 89, 93–94, https://doi.org/10.1029/2008EO100001, 2008.

Li, X., Xiao, Q., Niu, J., Dymond, S., McPherson, E. G., van Doorn, N., Yu, X., Xie, B., Zhang, K., and Li, J.: Rainfall interception by tree crown and leaf litter: An interactive process, Hydrological Processes, 31, 3533–3542, https://doi.org/10.1002/hyp.11275, 2017.

Longoni, L., Ivanov, V. I., Brambilla, D., Radice, A., and Papini, M.: Analysis of the temporal and spatial scales of soil erosion and transport in a Mountain Basin, Italian Journal of Engineering Geology and Environment, 16, 17–30, https://doi.org/10.4408/IJEGE.2016-02.O-02, 2016.

López Vicente, M., Pérez-Bielsa, C., López-Montero, T., Lambán, L. J., and Navas, A.: Runoff simulation with eight different flow accumulation algorithms: Recommendations using a spatially distributed and open-source model, Environ. Model. Softw., 62, 11–21, 2014.

Luino, F.: Sequence of instability processes triggered by heavy rainfall in the Northern Italy, Geomorphology, 66, 13–39, https://doi.org/10.1016/j.geomorph.2004.09.010, 2005.

Ly, S., Charles, C., and Degre, A.: Different methods for spatial interpolation of rainfall data for operational hydrology and hydrological modeling at watershed scale. A review, Biotechnology, Agronomy and Society and Environment, 17, 392–406, 2013.

Marnezy, A.: Alpine dams. From hydroelectric power to artificial snow, Revue de géographie alpine, 96, 2008.

Meisina, C., Zizioli, D., and Zucca, F.: Methods for Shallow Landslides Susceptibility Mapping: An Example in Oltrepo Pavese, 1, 451–457, https://doi.org/10.1007/978-3-642-31325-7-58, 2013.

Merritt, W. S., Letcher, R. A., and Jakeman, A. J.: A review of erosion and sediment transport models, Environmental Modelling & Software, 18, 761–799, https://doi.org/10.1016/S1364-8152(03)00078-1, 2003.

Milanesi, L., Pilotti, M., Clerici, A., and Gavrilovic, Z.: Application of an improved version of the Erosion Potential Method in Alpine areas, Italian Journal of Engineering Geology and Environment, https://doi.org/10.4408/IJEGE.2015-01.O-02, 2015.

Milledge, D. G., Bellugi, D., McKean, J. A., Densmore, A. L., and Dietrich, W. E.: A multidimensional stability model for predicting shallow landslide size and shape across landscapes, Journal of Geophysical Research: Earth Surface, 119, 2481–2504, https://doi.org/10.1002/2014JF003135, 2014.

Mishra, S. K., Tyagi, J. V., and Singh, V. P.: Comparison of infiltration models, Hydrological Processes, 17, 2629–2652, https://doi.org/10.1002/hyp.1257, 2003.

Moges, E., Demissie, Y., Larsen, L., and Yassin, F.: Review: Sources of Hydrological Model Uncertainties and Advances in Their Analysis, Water, 13, https://doi.org/10.3390/w13010028, 2021.

Montrasio, L.: Stability of soil-slip, Wit Press, Risk Analysis II, 45, 357–366, https://doi.org/10.2495/RISK000331, 2008.

Montrasio, L. and Valentino, R.: Modelling Rainfall-induced Shallow Landslides at Different Scales Using SLIP - Part II, Procedia Engineering, 158, 482–486, https://doi.org/10.1016/j.proeng.2016.08.476, 2016.

Morbidelli, R., Corradini, C., Saltalippi, C., Flammini, A., Dari, J., and Govindaraju, R. S.: Rainfall Infiltration Modeling: A Review, Water, 10, https://doi.org/10.3390/w10121873, 2018.

Morgan, R. P. C. and Nearing, M. A.: Handbook of erosion modelling., 2011.

Munich Re: Natural disasters caused overall losses of US $ 210bn Relevant natural catastrophe loss events worldwide 2020, 1, 2021.

Nazari, M., Sadeghi, S. M. M., Van Stan, J., and Chaichi, M.: Rainfall interception and redistribution by maize farmland in central Iran, Journal of Hydrology: Regional Studies, 27, 100656, https://doi.org/10.1016/j.ejrh.2019.100656, 2019.

Nino, Y.: Simple Model for Downstream Variation of Median Sediment Size in Chilean Rivers, Journal of Hydraulic Engineering, 128, 934–941, 2002.

Pacina, J., Lenďáková, Z., Štojdl, J., Matys Grygar, T., and Dolejš, M.: Dynamics of Sediments in Reservoir Inflows: A Case Study of the Skalka and Nechranice Reservoirs, Czech Republic, ISPRS International Journal of Geo-Information, 9, https://doi.org/10.3390/ijgi9040258, 2020.

Panagos, P., Borrelli, P., Poesen, J., Ballabio, C., Lugato, E., Meusburger, K., Montanarella, L., and Alewell, C.: The new assessment of soil loss by water erosion in Europe, Environmental Science & Policy, 54, 438–447, https://doi.org/10.1016/j.envsci.2015.08.012, 2015.

Papini, M., Ivanov, V., Brambilla, D., Arosio, D., and Longoni, L.: Monitoring bedload sediment transport in a pre-Alpine river: An experimental method, Rendiconti Online della Società Geologica Italiana, 43, 57–63, https://doi.org/10.3301/ROL.2017.35, 2017.

Pearson, E., Smith, M. W., Klaar, M. J., and Brown, L. E.: Can high resolution 3D topographic surveys provide reliable grain size estimates in gravel bed rivers?, Geomorphology, 293, 143–155, https://doi.org/10.1016/j.geomorph.2017.05.015, 2017.

Pebesma, E. J., de Jong, K., and Briggs, D.: Interactive visualization of uncertain spatial and spatio-temporal data under different scenarios: an air quality example, null, 21, 515–527, https://doi.org/10.1080/13658810601064009, 2007.

Peirce, S., Ashmore, P., and Leduc, P.: Evolution of grain size distributions and bed mobility during hydrographs in gravel-bed braided rivers, Earth Surface Processes and Landforms, 44, 304–316, https://doi.org/10.1002/esp.4511, 2019.

Pelletier, J. D., Broxton, P. D., Hazenberg, P., Zeng, X., Troch, P. A., Niu, G.-Y., Williams, Z., Brunke, M. A., and Gochis, D.: A gridded global data set of soil, intact regolith, and sedimentary deposit thicknesses for regional and global land surface modeling, Journal of Advances in Modeling Earth Systems, 8, 41–65, https://doi.org/10.1002/2015MS000526, 2016.

Pereira, S., Garcia, R., Zêzere, J., Oliveira, S., and Silva, M.: Landslide quantitative risk analysis of buildings at the municipal scale based on a rainfall triggering scenario, Geomatics, Natural Hazards and Risk, 8, https://doi.org/10.1080/19475705.2016.1250116, 2016.

Pérez-Peña, J. V., Azañón, J. M., and Azor, A.: CalHypso: An ArcGIS extension to calculate hypsometric curves and their statistical moments. Applications to drainage basin analysis in SE Spain, Computers & Geosciences, 35, 1214–1223, 2009.

Rahardjo, H., Satyanaga, A., Leong, E. C., Santoso, V. A., and Ng, Y. S.: Performance of an instrumented slope covered with shrubs and deep-rooted grass, Soils and Foundations, 54, 417–425, https://doi.org/10.1016/j.sandf.2014.04.010, 2014.

Ravi, V., Williams, J. R., and Ouyang, Y.: Estimation of infiltration rate in the vadose zone: compilation of simple mathematical models, 1998.

Raziei, T. and Pereira, L.: Estimation of ETo with Hargreaves-Samani and FAO-PM temperature methods for a wide range of climates in Iran, Agricultural Water Management, 121, 1–18, https://doi.org/10.1016/j.agwat.2012.12.019, 2013.

Remondo, J., Bonachea, J., and Cendrero, A.: A statistical approach to landslide risk modelling at basin scale: From landslide susceptibility to quantitative risk assessment, Landslides, 2, 321–328, https://doi.org/10.1007/s10346-005-0016-x, 2005.

Rickenmann, D.: Empirical Relationships for Debris Flows, Natural Hazards, 19, 47–77, https://doi.org/10.1023/A:1008064220727, 1999.

Rocha, J., Duarte, A., Silva, M., Fabres, S., Vasques, J., Revilla-Romero, B., and Quintela, A.: The Importance of High Resolution Digital Elevation Models for Improved Hydrological Simulations of a Mediterranean Forested Catchment, Remote Sensing, 12, https://doi.org/10.3390/rs12203287, 2020.

Ronchetti, F., Borgatti, L., Cervi, F., C, G., Piccinini, L., Vincenzi, V., and Alessandro, C.: Groundwater processes in a complex landslide, northern Apennines, Italy, Natural Hazards and Earth System Sciences, 9, 895–904, https://doi.org/10.5194/nhess-9-895-2009, 2009.

Roo, A., A.P.J, Wesseling, C. G., Jetten, V. G., and Ritsema, C.: LISEM: A physically-based hydrological and soil erosion model incorporated in a GIS, In: K. Kovar & H.P. Nachtnebel (eds.), Application of geographic information systems in hydrology and water resources management. Wallingford (UK), IAHS, 1996. IAHS Publ. 235, pp. 395-403, 1996.

Ross, C. W., Prihodko, L., Anchang, J., Kumar, S., Ji, W., and Hanan, N. P.: HYSOGs250m, global gridded hydrologic soil groups for curve-number-based runoff modeling, Sci Data, 5, 180091–180091, https://doi.org/10.1038/sdata.2018.91, 2018.

Salles, T.: eSCAPE: Regional to global scale landscape evolution model v2. 0, 2019.

Sambrook Smith, G. H. and Ferguson, R. I.: The gravel-sand transition along river channels, Journal of Sedimentary Research, 65, 423–430, https://doi.org/10.1306/D42680E0-2B26-11D7-8648000102C1865D, 1995.

Scheidl, C. and Rickenmann, D.: TopFlowDF - A simple gis based model to simulate debris-flow runout on the fan, https://doi.org/10.4408/IJEGE.2011-03.B-030, 2011.

Schellekens, J., Verseveld, W. van, Visser, M., hcwinsemius, laurenebouaziz, tanjaeuser, sandercdevries, cthiange, hboisgon, DirkEilander, DanielTollenaar, aweerts, Baart, F., Pieter9011, Pronk, M., arthur-lutz, ctenvelden, Imme1992, and Jansen, M.: openstreams/wflow: Bug fixes and updates for release 2020.1.2, Zenodo, https://doi.org/10.5281/zenodo.4291730, 2020.

Shobe, C., Tucker, G., and Barnhart, K.: The SPACE 1.0 model: A Landlab component for 2-D calculation of sediment transport, bedrock erosion, and landscape evolution, Geoscientific Model Development Discussions, 1–38, https://doi.org/10.5194/gmd-2017-175, 2017.

Sklar, L. S., Riebe, C. S., Marshall, J. A., Genetti, J., Leclere, S., Lukens, C. L., and Merces, V.: The problem of predicting the size distribution of sediment supplied by hillslopes to rivers, Geomorphology, 277, 31–49, 2017.

Smith, R. E. and Parlange, J.-Y.: A parameter-efficient hydrologic infiltration model, Water Resources Research, 14, 533–538, https://doi.org/10.1029/WR014i003p00533, 1978.

Strahler, A. N.: Dynamic basis of geomorphology, Geological society of america bulletin, 63, 923–938, 1952.

Strauch, R., Istanbulluoglu, E., Nudurupati, S. S., Bandaragoda, C., Gasparini, N. M., and Tucker, G. E.: A hydroclimatological approach to predicting regional landslide probability using Landlab, Earth Surf. Dynam., 6, 49–75, https://doi.org/10.5194/esurf-6-49-2018, 2018.

Sutanudjaja, E. H., van Beek, R., Wanders, N., Wada, Y., Bosmans, J. H. C., Drost, N., van der Ent, R. J., de Graaf, I. E. M., Hoch, J. M., de Jong, K., Karssenberg, D., López López, P., Peßenteiner, S., Schmitz, O., Straatsma, M. W., Vannametee, E., Wisser, D., and Bierkens, M. F. P.: PCR-GLOBWB 2: a 5\,arcmin global hydrological and water resources model, Geoscientific Model Development, 11, 2429–2453, https://doi.org/10.5194/gmd-11-2429-2018, 2018.

Takahashi, T.: A Review of Japanese Debris Flow Research, International Journal of Erosion Control Engineering, 2, https://doi.org/10.13101/ijece.2.1, 2009.

Tangi, M., Schmitt, R., Bizzi, S., and Castelletti, A.: The CASCADE toolbox for analyzing river sediment connectivity and management, Environmental Modelling & Software, 119, 400–406, https://doi.org/10.1016/j.envsoft.2019.07.008, 2019.

Tavares da Costa, R., Mazzoli, P., and Bagli, S.: Limitations Posed by Free DEMs in Watershed Studies: The Case of River Tanaro in Italy, Frontiers in Earth Science, 7, 141, https://doi.org/10.3389/feart.2019.00141, 2019.

Terzago, S., Palazzi, E., and von Hardenberg, J.: Stochastic downscaling of precipitation in complex orography: a simple method to reproduce a realistic fine-scale climatology, Nat. Hazards Earth Syst. Sci., 18, 2825–2840, https://doi.org/10.5194/nhess-18-2825-2018, 2018.

Theule, J.: Geomorphic study of sediment dynamics in active debris-flow catchments (French Alps), 2012.

Tóth, B., Weynants, M., Pásztor, L., and Hengl, T.: 3D soil hydraulic database of Europe at 250 m resolution, Hydrological Processes, 31, 2662–2666, https://doi.org/10.1002/hyp.11203, 2017.

Tramblay, Y., Bouvier, C., Martin, C., Didon-Lescot, J.-F., Todorovik, D., and Domergue, J.-M.: Assessment of initial soil moisture conditions for event-based rainfall–runoff modelling, Journal of Hydrology, 387, 176–187, https://doi.org/10.1016/j.jhydrol.2010.04.006, 2010.

Uber, M., Vandervaere, J.-P., Zin, I., Braud, I., Heistermann, M., Legoût, C., Molinié, G., and Nord, G.: How does initial soil moisture influence the hydrological response? A case study from southern France, Hydrology and Earth System Sciences, 22, 6127–6146, https://doi.org/10.5194/hess-22-6127-2018, 2018.

Vakhshoori, V. and Zare, M.: Is the ROC curve a reliable tool to compare the validity of landslide susceptibility maps?, null, 9, 249–266, https://doi.org/10.1080/19475705.2018.1424043, 2018.

Van Der Knijff, J. M., Younis, J., and De Roo, A. P. J.: LISFLOOD: a GIS-based distributed model for river basin scale water balance and flood simulation, null, 24, 189–212, https://doi.org/10.1080/13658810802549154, 2010.

Van Genuchten, M.: A Closed-form Equation for Predicting the Hydraulic Conductivity of Unsaturated Soils1, Soil Science Society of America Journal, 44, https://doi.org/10.2136/sssaj1980.03615995004400050002x, 1980.

de Vente, J. and Poesen, J.: Predicting soil erosion and sediment yield at the basin scale: Scale issues and semi-quantitative models, Earth-Science Reviews, 71, 95–125, https://doi.org/10.1016/j.earscirev.2005.02.002, 2005.

Vetsch, D., Siviglia, A., Caponi, F., Ehrbar, D., Gerke, E., Kammerer, S., Koch, A., Peter, S., Vanzo, D., Vonwiller, L., Facchini, M., Gerber, M., Volz, C., Farshi, D., Mueller, R., Rousselot, P., Veprek, R., and Faeh, R.: System Manuals of BASEMENT Version 2.8, 2018.

Vitvar, T., Burns, D. A., Lawrence, G. B., McDonnell, J. J., and Wolock, D. M.: Estimation of baseflow residence times in watersheds from the runoff hydrograph recession: method and application in the Neversink watershed, Catskill Mountains, New York, Hydrological Processes, 16, 1871–1877, https://doi.org/10.1002/hyp.5027, 2002.

Yu, B., Xie, C., Cai, S., Chen, Y., Lv, Y., Mo, Z., Liu, T., and Yang, Z.: Effects of Tree Root Density on Soil Total Porosity and Non-Capillary Porosity Using a Ground-Penetrating Tree Radar Unit in Shanghai, China, Sustainability, 10, https://doi.org/10.3390/su10124640, 2018.

Zhang, H., Li, Z., Saifullah, M., Li, Q., and Li, X.: Impact of DEM Resolution and Spatial Scale: Analysis of Influence Factors and Parameters on Physically Based Distributed Model, Advances in Meteorology, 2016, 8582041, https://doi.org/10.1155/2016/8582041, 2016.

Zomlot, Z., Verbeiren, B., Huysmans, M., and Batelaan, O.: Spatial distribution of groundwater recharge and base flow: Assessment of controlling factors, Journal of Hydrology: Regional Studies, 4, 349–368, https://doi.org/10.1016/j.ejrh.2015.07.005, 2015.